Vacuum 179 (2020) 109545

Contents lists available at ScienceDirect

Vacuum

journal homepage: http://www.elsevier.com/locate/vacuum

A review on hot cathode ionisation gauges with focus on a suitable design for measurement accuracy and stability

Karl Jousten [a,*], Frederic Boineau [b], Nenad Bundaleski [c], Claus Illgen [a], Janez Setina [d], Orlando M.N.D. Teodoro [c], Martin Vicar [e], Martin Wüest [f]

[a] Physikalisch-Technische Bundesanstalt (PTB), Abbestr. 2-12, 10587, Berlin, Germany
[b] LNE 1 rue Gaston Boissier, 75724, Paris Cedex 15, France
[c] CEFITEC, Department of Physics, Faculty of Sciences and Technology, Nova University of Lisbon, 2829-515, Caparica, Portugal
[d] IMT Institute of Metals and Technology, Lepi pot 11, 1000, Ljubljana, Slovenia
[e] Czech Metrology Institute (CMI), Okruzni 772/31, 638 00, Brno, Czech Republic
[f] INFICON AG, Alte Landstrasse 6, LI-9496, Balzers, Liechtenstein

ARTICLE INFO

Keywords:
Ionisation gauge
Hot cathode
Sensitivity
Secondary electrons
Electron stimulated desorption

ABSTRACT

A literature review starting from 1950 is given on the design and geometry of ionisation gauge types with hot cathodes. Considerations on the material of the electrodes and of surface effects are included. The review focuses on the design issues for measurement accuracy, linearity, repeatability, reproducibility, and stability of sensitivity. Also, the attempts to reduce the lower measurement limit are reviewed to some extent.

1. Introduction

The ionisation gauge [1] is the measuring instrument for high and ultrahigh vacuum, and besides the rarely applicable spinning rotor gauge the only vacuum gauge type for this pressure range. For many applications such as the control of valve switching or residual pressure checks, the design and electrical equipment of ionisation gauges can be kept simple, because no high measurement accuracy is required. However, vacuum calibration laboratories including National Metrological Institutes and laboratories, which measure pumping speeds of high vacuum pumps, require ionisation gauges that offer a high measurement accuracy and long-term stability which is normally not achieved by commercial gauges. In addition, the ISO Technical Committee 112 for Vacuum Technology requested research for a standardized ionisation gauge suitable for calibration purposes with some emphasis on a stable relative gas sensitivity factor in the range from 10^{-6} Pa to 10^{-2} Pa.

The European project EMPIR 16NRM05 joining 5 National Metrological Institutes, CERN, the Nova University of Lisbon and two gauge manufacturers carry out such research. To this end, a review of the pertinent literature starting at a time, when the so-called Bayard-Alpert gauge (BAG) was invented, was undertaken which is presented in this report. The collection of papers contains more than 260 papers published from 1948 to 2017. This review focuses on subjects relevant for the project, i.e. a stable and robust sensitivity in the high vacuum range, in particular relative gas sensitivity factors.

The history of ionisation gauges dates back to 1909, when von Baeyer [2] showed that a triodic vacuum tube can be used as vacuum gauge. A few years later Buckley [3] presented the first ionisation gauge. For about 30 years the triode design remained unchanged until Bayard and Alpert developed a new gauge type [4] which significantly reduced the lower measurement limit of the triode type gauge (Fig. 1).

In ionisation gauges, either a controlled electron emission current from a hot cathode or a discharge current in a plasma is used for electron generation. The latter type is usually called “cold cathode (ionisation) gauge” or "crossed field ionisation gauge" as defined in ISO 3529–3:2014, the first “emitting cathode ionisation gauge” (ISO 3529–3:2014). Since the 1990s there were many attempts to replace the electron emitting hot cathode by a cold cathode using field electron emission from shaped Mo or Si devices or recently from carbon nanotubes. Up to now, none of the cold electron emitting cathodes have been a commercial success and so we still call ionisation gauges with an emissive cathode “hot cathode ionisation gauge” (HCIG) in this paper.

In the mentioned project we pursue only HCIG because of the nonlinearities present in crossed field ionisation gauges [5], which make

* Corresponding author.
E-mail address: karl.jousten@ptb.de (K. Jousten).

https://doi.org/10.1016/j.vacuum.2020.109545
Received 13 March 2020; Received in revised form 5 June 2020; Accepted 6 June 2020
Available online 10 June 2020

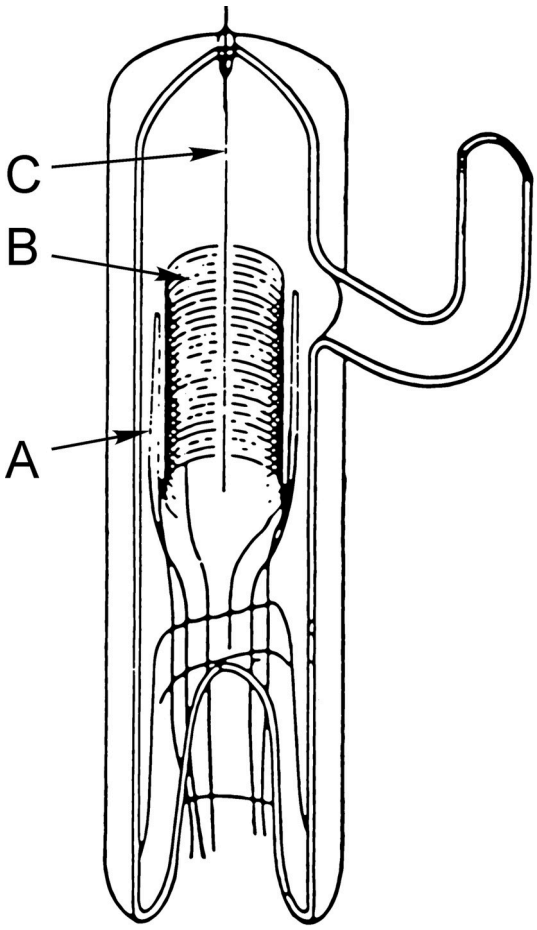

Fig. 1. The Bayard-Alpert gauge as designed by the authors in 1950 [4]. A: cathode; B: anode grid, C: collector.

it rather complicated and expensive to calibrate them.

The measured quantity in a HCIG is the current of ions I^+ produced by electron impact. Describing the main physical effect, I^+ is proportional to the electron current I_e, the mean effective path length L of the electrons, the ionisation cross section of the molecules by the electrons $\sigma_{E,gas}$, the capture probability $c_{ion,C}$ of the ions by the collector (Fig. 1) and finally the number density n_V of molecules in the ionisation gauge.

In more detail, the model equation that considers all the significant effects is (see also Fig. 10)

$$\begin{aligned} I^+ = {} & I_e\left(n_V + n_{gen} - n_{pumped}\right)\sigma_{E,gas} L c_{ion,C}\left(1+\gamma_{e,ion}\right) + k_A I_e n_S \sigma_S c_S \\ & + k_A I_e \gamma_{e,e}\left(n_V + n_{gen} - n_{pumped}\right)\sigma_{E^*,gas} L^* c_{ion,C} + I_e k_{x,A} c_{X,C} \gamma_{e,X,C} \\ & - I_e k_{X,W} \gamma_{e,X,W} c_{X,W} + I_{leak} \end{aligned} \quad (1)$$

The symbols are explained in Table 1. The first term describes the current of ions captured by the collector and produced by the primary electrons, enhanced by secondary electrons from the ion impact on the collector. The second represents ions desorbed from the anode and captured by the collector. The third quantifies captured ions produced when secondary electrons from the anode ionize neutral particles. The fourth describes electrons leaving the collector and generated by X-rays, the fifth electrons generated by X-rays drifting from the wall to the collector, the last term leakage current across insulators to the collector.

Among the neglected quantities of higher order effects in the formula are those related to electrons which are generated by the X-rays on the wall and on the collector which may gain enough energy to also ionize molecules.

This review structures the literature as follows:

- Principal design and geometry of the HCIG determining L, k_A, $k_{X,A}$, $k_{X,W}$, c_S, $c_{X,C}$, $c_{X,W}$ (Section 2)
- Electrode material determining n_S, $k_{x,A}$, $\gamma_{x,C(W)}$ (Section 3)
- Electrical supply (Section 4)
- Surface effects determining $\gamma_{e,ion}$, $\gamma_{e,X,C(W)}$, $\gamma_{e,e}$, n_{gen}, n_{pumped} including outgassing effects etc., but also $k_{X,A}$, n_S (Section 5)
- Sensitivity and stability (Section 6)
- Simulation of trajectories in ionisation gauges (Section 7)

A way to improve accuracy at the lower end of the measurement range is to reduce the lower measurement limit. This is included in Section 2.2.

For this review it is assumed that the reader is familiar with the principle design of hot cathode ionisation gauges. Introductions can be found in textbooks as e.g. Ref. [6]. ISO 27894 [1] explains the terms used in this paper. In order not to cause confusion with the referenced data material, we will use the units of the original literature. It is 1 Torr = 1,33322 mbar = 133,322 Pa.

2. Design and geometry

Surprisingly, in the 1960s very few papers discussed the geometry of BAGs or other HCIGs, and even fewer made a systematic investigation of how the position of electrodes would change the sensitivity. We present this part of the review mainly in chronological order.

2.1. General design

A paper by Baker and Yarwood [7] in 1957 reported on an early modification of the BAG by closing the open cylindrical anode grid at the two ends and adding a shield around the grid anode. This shield has a negative potential compared to the cathode and increases the number of electrons that take part in the ionisation process (I_e in Eq. (1)). The first modification increases $c_{ion,C}$ in Eq. (1). Both methods increase sensitivity, but only the first one has some positive effect on the stability, because less ions are susceptible to be lost by incidents due to scattering, space charge, change of emission point etc.

In 1961 Redhead [8] described the reduction of the residual current in the BAG to an equivalent of 10^{-11} mbar by reducing the collector wire diameter to 25 μm. For lower pressures, the instability and uncertainty of the residual current I_r, may cause instabilities and uncertainties of the measured pressure. I_r can be measured by varying the grid potential: The idea is that more X-rays are generated with higher grid voltage. He mentioned, however, that this measurement is unreliable, because also the electron stimulated desorption changes as well as the pumping speed of the gauge.

The first systematic theoretical and experimental investigation on the geometry of the BAG was carried out in 1962 by Schütze [9]. By theoretical considerations he showed that the sensitivity depends on the product of grid diameter d_g and the ratio ρ of grid diameter to collector diameter (Fig. 2). When $\rho > 100$ (which is for a collector diameter of 100 μm happening at $d_g = 10$ mm), the sensitivity becomes independent of the ratio ρ and is therefore proportional to d_g. The latter is the case for most commercial BAGs.

Schütze also investigated experimentally the role of the diameter of the grid, the thickness (diameter) of the wire forming the anode grid and the lead (pitch height) of the grid. The experimental dependence of the sensitivity from the grid diameter was a bit weaker than linear as expected from a simplified theory. There was a monotonic decrease of the sensitivity with the wire thickness. For $d_g = 15$ mm, it dropped by almost 20% from a wire thickness of 0.15 mm to the one of 0.4 mm. This can be explained by the fact that the thicker the wire the more electrons will hit the grid at their first pass and be kept away from the ionisation area. For the same reason the sensitivity increases strongly with increasing wire lead from 1 mm to 2 mm, but for a wire thickness and $d_g = 15$ mm reaches a weak maximum at 3 mm, where after the sensitivity drops

Table 1
Symbols and quantities used in Eq. (1) to describe the measured ion current in a hot-cathode ionisation gauge.

Symbol	SI unit	Quantity	Comment
I^+	A	Measured ion current by the controller	
I_e	A	Effective electron current entering the ionisation region	The effective electron current may differ from the measured one in the emission circuit or in the anode circuit. It includes backscattered electrons from anode grid.
I_{leak}	A	Leakage current from another electrode	Should be zero
n_V	m^{-3}	Number density (per volume) of neutral molecules that diffuse into the ionisation space from the chamber	
n_{gen}	m^{-3}	Number density (per volume) of neutral molecules that are generated by the gauge itself	Additional molecules in the gauge can be generated by thermal outgassing, by fragmentation by electron impact or at the hot cathode, or by electron stimulated desorption from surfaces
n_{pumped}	m^{-3}	Number density (per volume) of neutral molecules that are removed from n_V by pumping effects of the gauge	Only pumping effect by surface adsorption, not ion implantation (these ions were counted already)
$\sigma_{E,gas}$	m^{-2}	Ionisation cross section for molecules of species "gas" by electrons with energy E (respectively E')	E is the electron energy averaged along the part of their trajectories inside the ionisation space. E' is the electron energy of inelastically scattered electrons or secondary electrons from the anode.
L	m	Mean path length of an electron from the emitter in the ionisation space	The ionisation space is defined as the volume where the generated ions can reach the ion collector. The path length can be increased by electrons elastically backscattered at the anode or by magnetic fields.
$c_{ion,C}$	1	The probability that the ion is captured by the collector	The reference number are the ions in the ionisation space as defined above.
$\gamma_{e,ion}$	1	The mean number of secondary electrons produced when an ion hits the collector	This number depends on the ion species, ion energy, the collector material, its surface, and the angle of the hit
$\gamma_{e,e}$	1	The mean number of secondary electrons able to ionize gas molecules, produced when an electron hits the anode	This number depends on electron energy, the collector material, its surface, and the angle of the hit. Only secondary electrons with enough energy to ionize are counted.
k_A	1	The fraction of the electron current hitting the anode	
n_S	m^{-2}	Number density (per surface area) of molecules on the surface of the anode	
σ_S	m^{-2}	Ionisation cross section for molecules on the surface by electrons with energy E	Causes electron stimulated desorption (ESD) of ions
c_S	1	The probability that the desorbed ion (see above) is captured by the collector	
L'	m	Mean path length of an electron backscattered from the grid or of a secondary electron from the grid in the ionisation space	
$k_{X,A}$	1	The number of X-ray photons produced per electron hitting the anode	
$c_{X,C}$	1	The probability that the X-ray photon (from the anode) hits the collector	Causes the "X-ray" limit
$\gamma_{e,X,C\,(W)}$	1	The mean number of secondary electrons produced when the X-ray photon hits the collector (wall)	
$k_{X,W}$	1	The number of X-ray photons hitting the wall produced per electron hitting the anode	
$c_{X,W}$	1	The probability that the electron from the wall reaches the collector	Causes the inverse "X-ray" effect
I_r	A	Residual ion current which is independent of n_V	I_r is equal to I^+ when $n_V = 0$; not used in Eq. (1), but in literature and following text.

slightly. The reason for this is that the electrostatic field penetration from outside potentials through the grid wires gets larger for a too large lead and reduces the potential inside of the grid.

In addition, Schütze investigated the role of the collector position within the anode grid and the distance of emitting hot cathode (longitudinal wire parallel to anode axis, no hairpin) and anode. For the latter he found a 20% increase of sensitivity from 1 mm to 4 mm distance, where there was a maximum, and a slight decrease in sensitivity up to 10 mm distance (Fig. 11 b in Refs. [9]). He noticed that it is important to have a symmetrical arrangement of the cathode wire to the grid. The position of the collector was favourable in the centre of the grid, but no loss of sensitivity was observed when the collector was moved perpendicular to the plane spanned by the grid axis and the cathode. The longitudinal movement of the collector away from the cathode or towards it, however, decreased the sensitivity by about 25% (Fig. 11 a in Refs. [9]).

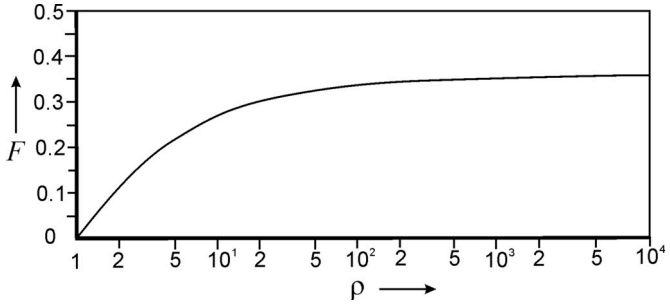

Fig. 2. The quantity F, which is proportional to sensitivity of a BAG, in dependence of $\rho = d_g/d_c$ with d_g grid and d_c collector diameter. From Fig. 6 in Ref. [9]. Used potentials were 0 V for the cathode, 150 V for the anode grid, −30 V for the collector.

Groszkowski, from about 1965 to 1970, was the next researcher who made systematic investigations on the influence of electrode dimensions on the BAG sensitivity [10–16]. He found that the sensitivity decreases monotonically by about a factor of 10 when the collector diameter d_c was changed from 2 mm to 9 μm [16]. The reduction of sensitivity is explained by a reduced ion collection efficiency $c_{ion,C}$ due to the higher angular momentum of the ions. This experimentally measured reduction of sensitivity is somewhat weaker than indicated by theoretical considerations of Comsa [17].[1] Comsa explained this fact that Groszkowski worked with residual gases, which contain an important number of diatomic molecules. These molecules, being ionized, give birth to ions which have velocities corresponding not only to the thermal energy (0.026 eV), but also to energies up to 1 eV and higher. Higher energies (higher angular momentum) lead to lower capture probability by the collector. Benvenuti [18] found that the influence of d_c is weaker, when the anode grid is closed. The sensitivity decreased for the closed grid

[1] In this way the advantage of X-ray limit reduction has a drawback in the reduction of sensitivity.

only below 50 μm. Hseuh [19] reported a reduction of 30%, when the diameter was reduced from 125 μm to 50 μm.

Replacing the one collector wire by four parallel of the same kind forming a square prism did increase the sensitivity by 20% only [16]. Forming a thin wire into a helical one (0.15 mm wire into a helical diameter of 1 mm with 6 turns per 1 mm) gave the same sensitivity as a 1 mm wire [16].

The sensitivity also increased with the length of the collector wire, with the larger effect for bigger diameters [16]. The collector position in the centre of the anode gave the maximum sensitivity [12,16].

The sensitivity is about linearly proportional to the grid diameter d_g, hence also L. However, a large diameter (40 mm) with at the same time small length (5 mm) appeared unfavourable [16]. The diameter should not exceed 6 times the length of the grid. Closed grids prevent generated ions to escape from the ionisation volume and therefore increase sensitivity up to a factor of 4, depending on the collector diameter [11, 17,20].

For the cathode – anode distance Groszkowski found a weak increase of 20% in sensitivity, when this distance was varied from 1 mm to 15 mm, which is somewhat different from the results of Schütze (he used a longitudinal wire, not hairpin as cathode) described above and in contradiction of a finding by Redhead [21], see below. Also, length and position of the cathode (the emission current was kept constant at 4 mA) along the anode axis had a very weak influence on the sensitivity.

Groszkowski also estimated the number of oscillations of the electrons and found 2 to 4 oscillations, where the higher number is true for smaller grid wire diameters [16].

Redhead [21] found an increase in sensitivity by a factor of 2.5, when the hairpin cathode was moved radially away from the anode grid of a BAG from 0.5 mm to 6 mm distance. A similar strong dependence on L_{gf} (grid-filament distance) was also found by Nottingham [22]. A shield around the cathode opposite to the anode reduced this dependence on grid-cathode distance L_{gf} significantly for $L_{gf} > 3$ mm [21].

Bills et al. [23] stated in 1984 that the main cause of inaccurate and unstable sensitivities in BAG is the unstable and nonreproducible distribution of electron emission from hot cathodes. To this end, they defined 4 requirements for a design of a stable BAG:

a. All emitted electrons must enter the ionisation space
b. Path length L (Eq. (1)) and energy of each electron must be independent of the point of origin on the cathode
c. The number of transits through the ionisation space must be constant (preferably 1)
d. The ion collection efficiency must be independent of the point of origin on the cathode

To meet these requirements Bills et al. [23] designed an interesting BAG shown in Fig. 3. A semi-circular ribbon as cathode is positioned in front of a slit of slightly deformed hemispherical anode grid. All electrons emitted from this ribbon take the same type of path and therefore length and have almost the same energy so that any changes of emission will not affect the sensitivity. In a modified design the authors proposed an exit slit for the electrons on the opposite side of the ribbon so that the electrons hit the outer part of the grid. In this way, the X-rays could not reach the ion collector directly. This design idea never made it into a series product due to materials of construction and sputtering effects reducing lifetime as the authors of this review learned from co-author Arnold in an email exchange.

Ten years later, Bills [24] investigated the causes of instabilities of ion collector current in glass tube BAGs by means of simulations using the software SIMION. He did not publish quantitative results but showed examples of electron trajectories. He studied the effects of changes in distance of cathode to anode, position of ion collector within the anode and the size of the gauge port. Bills also stated that the cause of sensitivity reduction at higher pressure is due to the ion space charge around the collector.

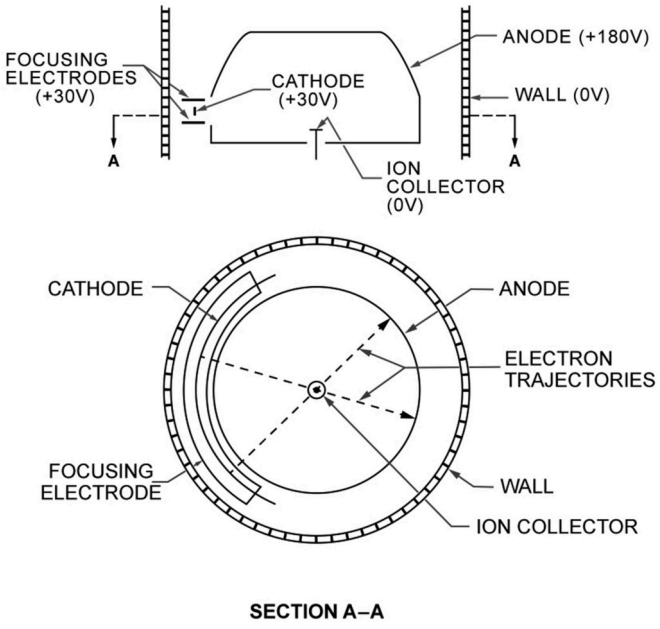

Fig. 3. The design idea by Bills et al. [23] to have identical path lengths of electrons independent of their origin. From. Reproduced from Fig. 2 in Refs. [23], with the permission of the American Vacuum Society.

Suginuma and Hirata investigated the influence of envelope diameter (35 mm–70 mm) on nude BAGs [25]. The sensitivities reduced by up to 40% for the largest diameter compared to the smallest. Filipelli [26] obtained similar results and found that the influence for the extractor gauges was less than from the BAGs. Also, Hseuh [18] confirmed that large envelope diameters (he increased up to 150 mm) reduce the sensitivity greatly (−45% from 35 mm to 150 mm).

As can be seen from Eq. (1), one important quantity of stability of sensitivity is the electron path length L. Peacock [27] made the point that the more passes the electrons make through the ionisation space the higher the risk of instability of the mean length. In a BAG, however, the mean number of passes is less than 2 (this can be estimated from the sensitivity and pressure normalised differential ionisation, see Eq. 13.32 in Ref. [6]) and a change of probability that an electron will make another pass through the ionisation space has no significant effect on L.

Another possibility of instability in L are unstable electron trajectories. Here, the emission cathode plays a very important role. Depending on where and by which angle the electron starts its trajectory on the cathode surface it will take different paths through the ionisation region and hit different parts of the anode grid. This was shown in an investigation by Jousten and Röhl [28], who combined two types of anodes with either cylindrically ordered rods or rings with two types of cathode emitters, hairpin or ring. From the four combinations it could be shown that the distribution of received electrons on the isolated parts of the anodes depend on time and treatments of the gauge like degassing, high pressure operation, exposure to CO_2 etc. As can be expected, the hairpin cathode made a quite unequal distribution of electrons on the anode. In the radial direction of the anode, the rods close to the hairpin and opposite to it received about 5 times more electrons than the ones with 90° to that line (see Fig. 4).

In the longitudinal direction the anode parts close to the curved end of the hairpin received almost 10 times more current than the lowest ring anode (see Fig. 6 in Ref. [28]).

The conclusion from this paper is that about 20% of the emitted electrons do not enter the ionisation space. About 5% (6% of the ones entering the ionisation space) of the total electron number have trajectories that fluctuate between distinct parts of the anode and their path length L easily changes by 10% causing a sensitivity change of 0.6%.

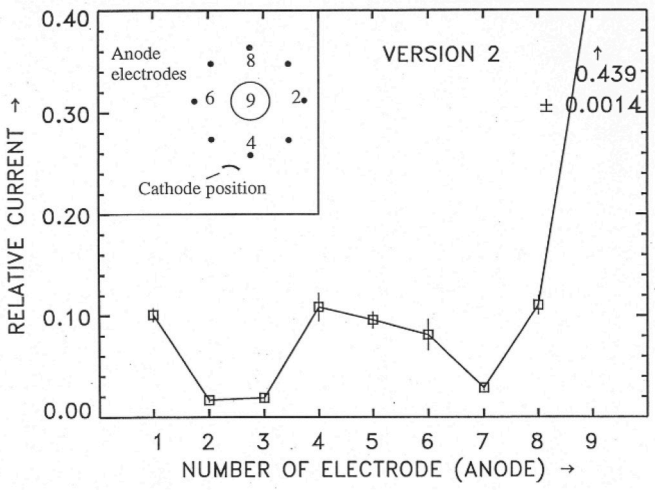

Fig. 4. Mean electron distribution captured by different rod electrodes of the anode in an extractor gauge. The bars show the 1σ variation of relative currents after typical gauge operations. Electrode 9 closes the grid as endplate. Reproduced from Fig. 5 in Ref. [28], with the permission of the American Vacuum Society.

To avoid the problem of an undefined electron trajectory within the ionisation gauge, Klopfer [28] designed a gauge with a straight electron path through the ionisation region (Fig. 5). The confinement of the electron beam was supported by a magnetic field of 1000 Gauss (0.1 T) along the axis of the beam.

He obtained a reasonable sensitivity of about 20 $mbar^{-1}$ with a path length of 15 mm and a good linearity. As electron trap served a simple plate ("T" in Fig. 5), but this caused reflected electrons and secondary electrons to reach the opposite electrode which made the electron signal current inaccurate.

An attempt to overcome the disadvantages of the BAG design causing instabilities was carried out by Sutton [30]. He used a triode design (Fig. 6) with the emitting cathode "F" in the centre of a cylindrical mesh grid "G" serving as anode. Different from the usual triode design, the collector "C" was another mesh cylinder or just a ring surrounding the anode. The mesh or ring greatly reduced the normally high X-ray limit of the triode design to about 10^{-6} Pa.

The sensitivity of this gauge was very stable (scatter of less than 1% within 850 h of operation), probably, because also here the electron path is quite well defined. The electrons move radially from the centre cathode through the cylindrical anode mesh to enter the effective ionisation space and are pushed back to the mesh by the collector or shield potential.

Triode gauges were also investigated by Hirata. He could attribute sensitivity changes on the electrode positions [31]. A radial movement of the filament cathode caused a sensitivity change of 4%/mm.

The perhaps most successful design to optimise the stability of a BAG undertook Arnold, Bills and Borichevsky with their development of the commercial STABIL–ION–Gauge by Granville Phillips [32–35]. They systematically analysed the weaknesses of commercial BAGs at that time [32] and provided for stable electrode positions including the ground potential surrounding the gauge. They also optimised the length of electron trajectories inside the ionisation volume and the stability of electron emission from the hot cathode. Special tools were prepared so that all components were always positioned in the same way.

2.2. *Designs to reduce the X-ray and the ESD limit*

Different constructions to reduce the X-ray limit are described in reviews by Redhead [36,37], including modulator gauge [38], spherical grid gauge, point collector gauge, bent-beam, axial and hemispherical gauges, extractor gauge, long electron path gauges and magnetic gauges. The idea of the point collector gauge [39] was not only to reduce the diameter of the collector but also its length visible to the X-rays. As explained in Ref. [36], experimental and theoretical conclusions show that reducing the collector diameter below 100 μm would result in a reduction of sensitivity as large as the reduction in the X-ray effect, thus

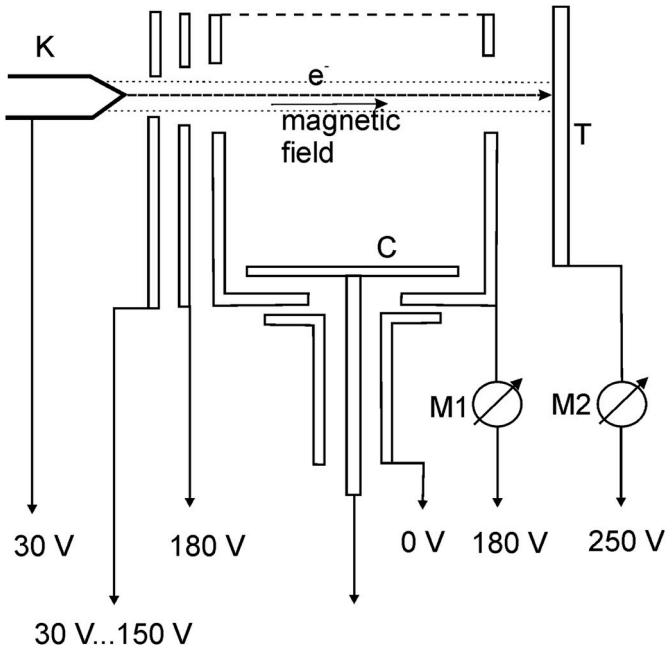

Fig. 5. Ionisation vacuum gauge by Klopfer [29]. K: cathode; C: ion collector; T electron trap. M2 measures electron current, by M1 the magnetic field was adjusted. The geometrical path length of the electrons through the anode cage was 15 mm. Reproduced from Ref. [29], with the permission of the American Vacuum Society.

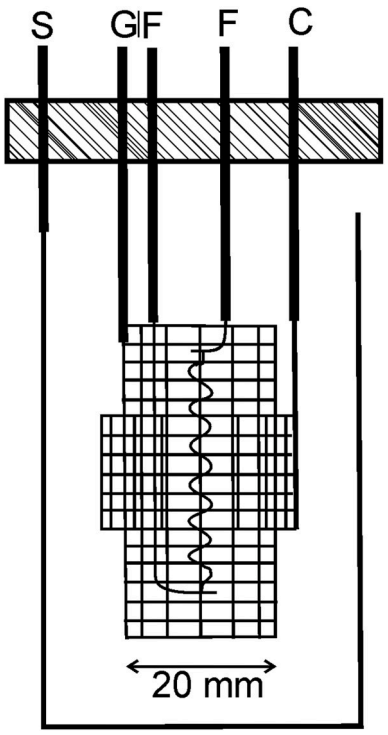

Fig. 6. Ionisation vacuum gauge by Sutton [30]. F filament, C collector, G grid, S screen.

causing a constant X-ray limit.

One of the widely used and commercially available UHV gauge is the extractor gauge [40] (Fig.7). The shape of a shield prevents the X-ray photons from the grid to directly impact the collector and, together with the reflector (using appropriate potential between the shield and reflector), focuses the ion beam onto the collector.

Another design of UHV gauge is called the Helmer gauge [41] (Fig. 8), popular for the measurement of very low pressures in the late 1960s until the 1980s. The ion beam is bent using an electrostatic field so that X-rays have no line of sight to the collector. In addition, a suppressor electrode was added to push back the secondary electrons, emitted from collector by X-rays or ions, onto the collector. The suppressor electrode is partly hit by the X-rays producing the reverse X-ray current to the collector [36,42]. The design enabled measurement down to 10^{-12} Pa.

The designs of the hidden collector as in the extractor and Helmer type are described in detail in Ref. [43] including the discussion and explanation of the wide spread properties for similar gauge designs; the efficiency of extracting ions is theoretically described depending on small changes in electrodes formation, shape and potential.

Overall, all extractor type gauges show better sensitivity for pressures below 10^{-8} Pa relative to the alternative, i.e. modulated BAGs [43], a special type of BAG to reduce its lower measuring range limit. An additional electrode, the modulator [44] served to modulate the ion current to the collector by changing the potential of the modulator between grid and collector potential to withdraw ions from the collector not affecting the path of X-rays at the same time. The differences of collector currents between the two potential states of the modulator should give the true ion collector current with the X-ray limit subtracted. The modulation, however, has some limitations reviewed in Ref. [45].

Besides the X-ray limit, electron stimulated desorbed (ESD) ions contribute to the residual ion current. To eliminate ESD ions, which have a higher energy than gas-phase ions (Fig. 9), Watanabe used an electrostatic analyser [46] (Fig. 9) or a modulator [47]. Also, by the extractor type HCIG and the Helmer type gauge ESD ions are suppressed [40]. Akimichi et al. [48] and Takahashi et al. [49] developed the so

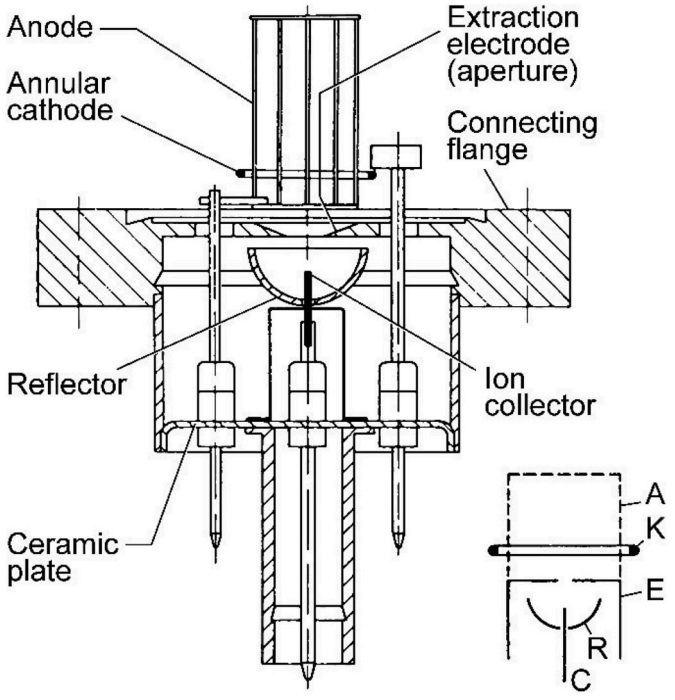

Fig. 7. Ionisation vacuum gauge of the extractor type [40]. Figure from Ref. [6]. Copyright Wiley-VCH Verlag GmbH & Co. KGaA. Reproduced with permission.

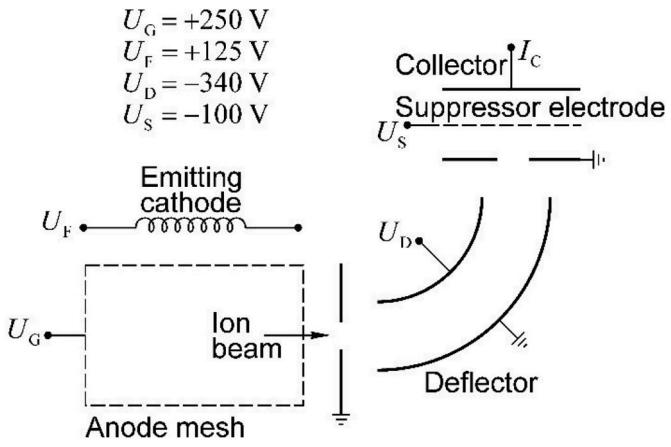

Fig. 8. Ionisation vacuum gauge of the Helmer type [41]. Figure from Ref. [6]. Copyright Wiley-VCH Verlag GmbH & Co. KGaA. Reproduced with permission.

called AxTran gauge with a Bessel box type analyser to suppress ESD, which is positioned on axis between ion source and ion collector and is therefore less bulky than Watanabe's design.

The intensity of reverse X-ray photocurrent (see Fig. 10 (e)) may be increased with keeping the potential of envelope approximately 20 V lower than collector potential [50]. In this way forward and reverse photocurrents can be balanced to an equal value, but the currents have opposite sign. Using identical materials at both photoemission surfaces stabilise this reduction.

There are several methods to measure the residual current I_r [51]:

1) Compare the collector current of the gauge with another gauge for which the residual current is either known or negligibly small. In Ref. [51], BAG and modulated gauges (MBAG) were compared to extractor gauges.
2) Modulation method using a modulator gauge
3) Increase the reflector voltage in an extractor gauge so that the ions will not reach the collector
4) Variation of electron energy method (VEE method), also called "Alpert method", first described in Ref. [4].

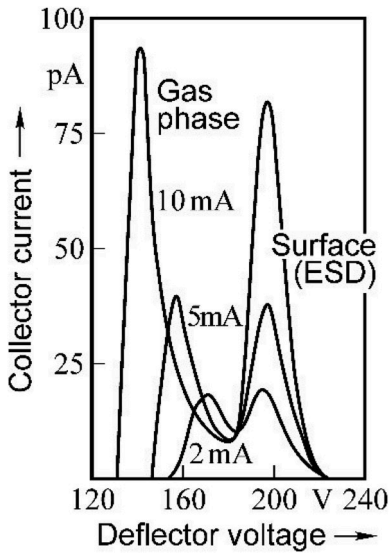

Fig. 9. Separation of ESD ions (O_2) from gas phase ions by energy in an ion spectroscopy gauge by Watanabe [46]. The separation is enhanced by space charge (higher emission currents). Figure from Ref. [6]. Copyright Wiley-VCH Verlag GmbH & Co. KGaA. Reproduced with permission.

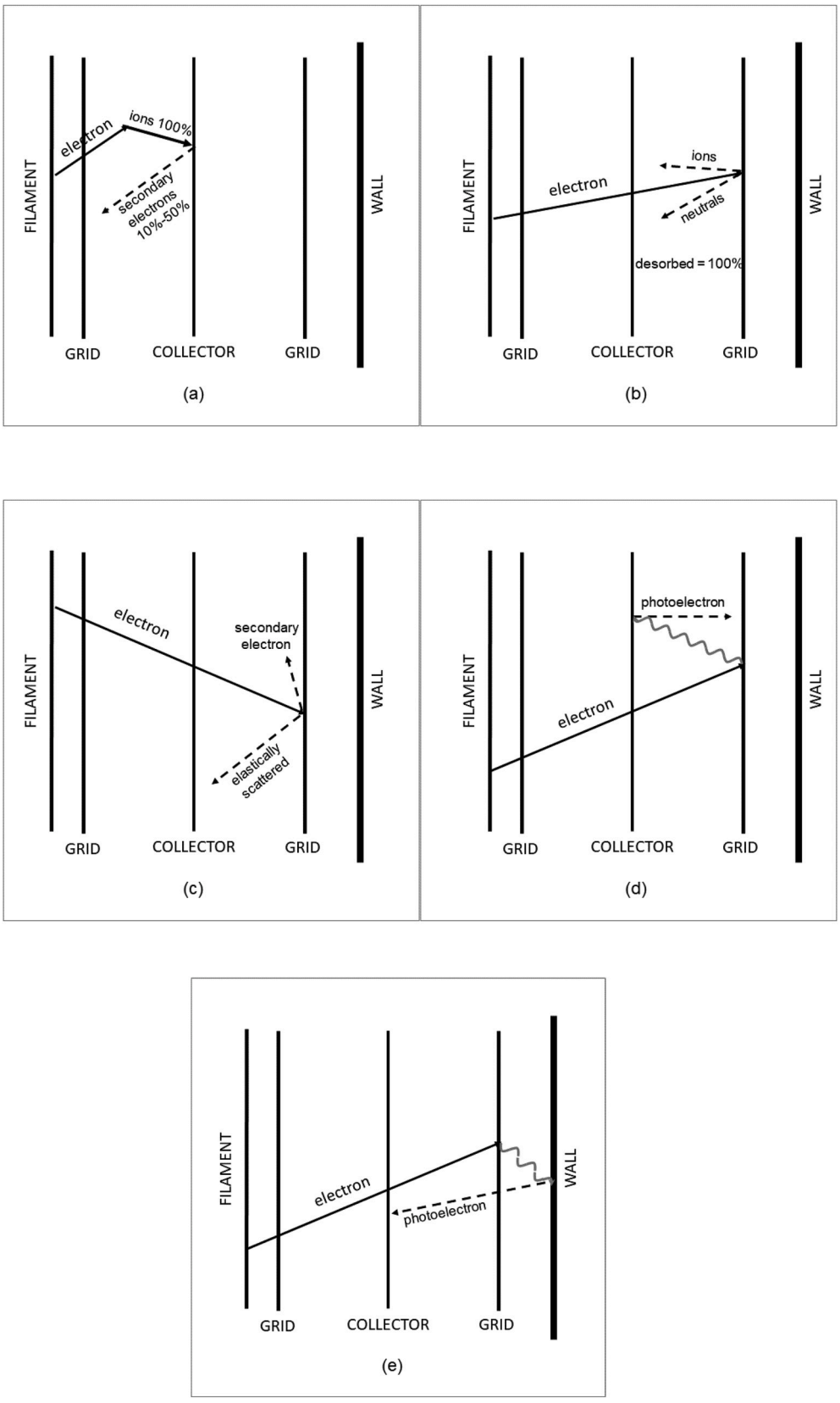

Fig. 10. Main types of surface phenomena in ionisation gauges for the example of Bayard-Alpert gauges; (a) Secondary electron emission from collector; (b) electron stimulated desorption of molecules; (c) Elastically backscattered electrons and electron induced secondary electron emission on grid; (d) X-ray effect; (e) inverse X-ray effect. Curved line: X-ray.

5) Reduce the pressure to extremely low value when gas phase ion current to collector is negligible. The estimated pressure for system partially immersed in liquid helium is 10^{-12} Pa [45].

To be able to vary the grid voltage (VEE method), the gauge must be operated with a special controller or power supply. The electrical feedthroughs must withstand operating voltages up to 1 kV. The experimental method is described in Ref. [52] together with comparison with X-ray limit estimated by comparison method (comparison with extractor gauge).

The VEE method of measuring residual current has been applied to many types of hot cathode gauges including the BAG. Measurements have been reported on suppressor gauges, extractor gauges and the point-collector gauges [45].

Several studies found the collector current versus filament to grid voltage curve to be made up of segments with different slopes. The breaks were attributed to the production of X-rays from new energy levels in the grid material as the electron energy increased.

3. Electrode materials

3.1. Electron emitting hot cathode

The main function of the cathode is the stable emission of electrons into the measuring volume. Mitsui [53] (1990) stated that the "thermionic emission from a metal is the typical electron source in ionisation pressure gauges and mass spectrometers."

The minimum amount of energy needed for an electron to leave a surface is called the work function. It is characteristic of a material (Table 2). Richardson used the work function W of the material for explaining the thermionic emission and proposed the emission law:

$$J = A_G T^2 e^{\frac{-W}{kT}} \tag{2}$$

J is the emission current density, k is the Boltzmann constant, T is the temperature and A_G is a parameter (Richardson constant) depending on the reflection of electrons at the material-vacuum surface and on the band structure of the emitting material.

Handbooks of the 1960s and 1970s [54,55] describe many aspects of the technology of hot cathodes, still valid today. Gear [56] (1975) explained effects influencing the electron emission. We summarize most of them, because they are concerning a stable emission:

General aspects [56]:

- Work function of a metal such as tungsten can be lowered by surface adsorption when atoms are adsorbed as positive ions
- Poisoning occurs when atoms are adsorbed as negative ions (electronegative contamination). In this case work function is increased resulting in a decrease in emission at a particular operating temperature. It can occur whenever oxidizing gases such as O_2, H_2O or CO_2 are present.

Table 2
The emission characteristics of various pure metals; only tungsten, tantalum and rhenium give useful emission levels [56]. Iridium was not mentioned in this paper.

\Metal	Melting point	Richardson constant A_G	Work function	Useable emitted current density
	K	A cm^{-2} K^{-2}	eV	A cm^{-2}
W	3640	80	4.54	0,4
Ta	3270	60	4.1	0,6
Re	3440	700	4.7	0,026
Mo	2890	55	4.15	0,005
Pt	2050	270	5.4	$2{\cdot}10^{-8}$
Ni	1730	60	4.1	$5{\cdot}10^{-9}$
Ba	1120	60	2.11	$1{\cdot}10^{-11}$

- Only tungsten, tantalum and rhenium give useful emission levels (Table 2)

These metals have the advantage that due to their high operating temperature contaminating electronegative gases which would increase work function and reduce emission levels are rapidly evaporated [57].

- A tungsten cathode can cause considerable changes in the gas composition of an ultra-high vacuum system [56,58,59].
- An ionisation gauge with tungsten acts as a pump [56], in particular for oxygen (producing WO, WO_2, WO_3)
- Tungsten wires contain alkali metals which can be thermally ionized at the hot surface [58] (heat treatment may avoid this)

Another important effect for the stability of sensitivity is the warpening of the hot cathode with time. Due to such geometrical changes the potential inside the gauge is altered and the position of the emitting surfaces. Both effects will change L.

In what follows, we summarize some important cathode effects [56]:

- Although possessing a lower work function and containing less carbon impurities than tungsten, tantalum is less suitable as a cathode material due to its adsorption properties for hydrogen.
- Rhenium has several advantages over tungsten as a cathode material. It is more resistant to water cycling and does not form stable nitrides and carbides. Hence oxygen interaction with carbon impurities produces less carbon monoxide. It does not become brittle at high temperatures and because of its hexagonal close-packed crystalline structure is an ideal base material for lanthanum hexaboride coatings. The high work function is a disadvantage as the self-evaporation rate is about 150 times higher than tungsten for the same emission level. The lifetime of a rhenium cathode is still long enough however to be useful in ionisation gauges.
- Iridium and rhodium are less suitable as cathode material, but extremely resistant to oxidation and are used as base materials in both thoriated and oxide coated cathodes.
- Among the refractory compounds such as the carbides, nitrides and borides, lanthanum hexaboride is the most important. It has a work function of 2.8 eV and gives adequate emission current at a temperature of 1400 K to be of use in ionisation gauges but is not suitable for UHV use due to the high sublimation rate.

Ions that are generated by electrons outside the anode grid may sputter the cathode. This may lead to minor geometrical changes, but also to changes in the working function, in particular on oxide coatings of the cathode.

Gasperic [60] (1967) described contamination with oil and other processes generating a carbon film on the cathode. He discovered a very simple method for the regeneration of such a cathode by heating it in oxygen.

For clean tungsten cathodes Angerth [61] (1974) measured a residual reading of about $1{\cdot}10^{-12}$ Torr at 10 mA emission. Similarly, Edelmann [62] found at 2400 K and 10 mA emission a vapour pressure of $4{\cdot}10^{-13}$ Torr and at 2200 K and 1 mA emission a vapour pressure of $8{\cdot}10^{-14}$ Torr. The measurement procedure of estimation this ion current for different cathode temperatures is described in Ref. [63], based on the grid potential modulation. The cathode evaporation limit in hot cathodes gauges can be eliminated by reducing the operating temperature of the cathode. The most effective method is to use a material with a low work function coating on the cathode such as thorium or yttrium [17,42,45].

Nemanic [64] reported about a pumping action of tungsten filaments for nitrogen and deuterium. The problem is critical in the case when the pumping speed of the main UHV pump is low.

Völter [65] used a LaB_6 cathode. He had to measure at oxygen pressures below $1{\cdot}10^{-6}$ Torr to avoid poisoning the LaB_6 cathode.

Dobrott [66] developed a SiC p-n junction "hot electron" emitter. The major disadvantage is the low level of emitted current in the 10^{-9} A range and imposed a low-pressure limit of 10^{-5} Torr.

Some authors [67,68] indicated that tungsten as cathode material provide better stability of the gauge sensitivity than a thoria coated iridium ribbon, but Arnold [32] suggested that the better stability is caused by using for tungsten a helical spring stretched between rigid supports. Such springs provide a better geometrical fixation of the electron emission area.

3.2. Collector electrode

Next to the cathode, the collector is a challenging electrode due to secondary electrons produced by the ion impingement ($\gamma_{e,ion}$ in Eq. (1)) which will be measured additively to the true ion current. This secondary electron yield depends on the surface of the collector.

Table 3 gives an overview of the materials reported for the collector.

Messer [75] recommended platinum and gold as a collector material for best long-term stability. One exception is when a platinum anode is used in the presence of hydrogen. The hydrogen will be absorbed by the platinum and later desorbed. When a massive gold collector was used, the sensitivity changed less than 1% in one year for noble gases and hydrogen and below 2% for oxygen, CO and CO_2 [76,77]. Also, Mitsui [52] used a collector made of a gold wire. Grosse [78] stated that the sensitivity is stable within 1% for gold and carbon but not for molybdenum where it varies by up to a factor of 2.

Thus, materials for which little changes in the chemical surface composition can be expected like gold and carbon should be preferred as grid and collector material (or coating of such).

3.3. Anode and other electrodes including envelope

To reduce the X-ray limit, a grid material which is relatively inefficient for the generation of X-rays (e.g., Pt or Pt–Ir alloy rather than W or Mo) [38] is helpful.

Molybdenum wire was used as anode grid by many researchers (see Table 3). It is very ductile and can be welded, brazed or rolled and can be connected to other materials without difficulties [79]. This material is also recommended for thermally stressed electrodes [79]. Molybdenum wires can be coated with a thin layer of gold, platinum or graphite for reducing the secondary emission from grids. Labrune [71] used a wire wound and a notched backbone made of molybdenum. Gentsch [81] modified the molybdenum grid with gold cladding.

Watanabe [82] used a grid formed by joining two hemispheres of fine woven molybdenum mesh spot-welded to tantalum rims.

Harten [77] reported a strong disadvantage of molybdenum. He found a very high yield of secondary electrons up to 0.1 from the molybdenum surface compared with 0.01 for tungsten, gold or carbon for electrons with 20 eV or more energy. For comparison, Harten [77] reported that in the case of carbon contamination the secondary electron emission of the gold coated tungsten anode remained relatively constant (within 1%) and at a low level ($\gamma_{e,e} = 0.2$).

Pittaway [43] used stainless-steel for the extractor electrode, reflector, and support wires. The modulator consisted of a tungsten wire.

Gentsch [76] reported about a platinum-iridium mesh anode at 300 °C. The measurements were performed with argon, the gauge coefficient of the BA gauge changed by about 1.4% during 3 years of observation.

Peters [69] used platinum wires as contacts against unwanted conduction cooling of the end parts of the tungsten filament.

In the commercial STABIL–ION–Gauge [34] a tantalum wire anode is used.

Fumio Watanabe [85] used a suppressor shield electrode located in front of the collector, covered with a very fine woven tungsten mesh (0.02-mm-diam wire, 50 mesh).

Tungsten is also used for springs for instance for giving the filament mechanical tension.

Watanabe [72] (1993) checked different gauge wall materials. At a low emission of 1 mA, an aluminium gauge wall had a very high pumping speed at UHV after degassing by electron bombardment. For a gold coated stainless steel wall, Watanabe [72] showed a low desorption. A reason may be the low emissivity for IR-radiation and the low reactivity of gold.

4. Electrical supply

Only few papers reported on the electrical supplies for ionisation gauges. The oldest supplies like the one from 1963 [86] were based on electron tubes.

The design of the ionisation gauge controller by Spencer and Staheli [87], which was published in 1968, is already based on semiconductor components. They give a complete circuit diagram for a BA gauge supply. Three basic voltage sources are required to operate HCIGs:

(i) a stable grid supply
(ii) a stable filament bias supply
(iii) a filament supply which is regulated to maintain a constant electron current to the grid.

In evaluation of the performance of a gauge with thorium coated filament they found that considerably more power is required to achieve the required emission current, if the filament is contaminated. Their controller achieved a stability of the grid current of 0.01% over a period of 16 h, for the cathode bias voltage of 0.01% and for the grid voltage of 0.2%.

In a more recent paper, Donkow and Knapp [88] discussed a problem of dynamic behaviour of BA controller in case of rapidly changing pressure in the vacuum system. An example of application is vapour rate measurements. They made a mathematical model of emission current controller and built one based on this model.

In glass envelope BA gauges, high frequency oscillations of electrons,

Table 3
Reported materials for different electrodes in hot cathode ionisation gauges.

Material	Collector	Anode	Extractor	Reflector	Modulator	Envelope or shield
tungsten	[33,34,43,69–72,83]				[21,43,84]	
tungsten gold coated	[77]					
nickel	[73],					
molybdenum	[78]	[13,47,69–71,77,79,80,82,83]		[47]		
molybdenum with gold or platinum clad		[81,111]				
stainless steel	[74]		[43]	[43]		
stainless steel gold coated						[72]
tantalum	[47]	[34]				[47]
platinum-iridium		[76,83]				
platinum	[48,75]	[83]				
gold	[32,75–78]					
carbon	[78]					
aluminium						[72]

known as Burkhausen-Kurtz oscillations occur [58]. The influence of the ionisation gauge electronics and supply leads on the oscillation damping was studied by Szwemin [89]. In the case of oscillations, he found 5%–10% increase of the ion current. A transparent conductive coating (tin oxide), deposited on the inner surface of the glass envelope almost completely reduces amplitude of Burkhausen-Kurtz oscillations [58,90].

In more recent times, Abbott and Looney [91] concluded in their paper that all electrically floating glass envelope BA gauge systems that use a.c. supply for cathode heating will exhibit a pressure dependent sensitivity. This nonlinearity can be minimized by using a controller that provides a noise free d.c. filament heating current.

For a stable gauge, all surfaces around electron beam should have well defined potentials, so they must be metallic. All insulators which can accumulate static charge should be shielded from direct impact of charged particles.

5. Surface effects

Four main types of surface phenomena affect the accuracy of vacuum pressure measurement with ionisation gauges [92] (Fig. 10):

1. Ion induced secondary electron emission from the collector of HCIGs ("a" in Fig. 10). This enhancement factor for the ion induced secondary electron yield (IISEY) is described by $(1+\gamma_{e,ion})$ in Eq. (1). Existence of IISEY is not a stability problem by itself, if it is constant. However, $\gamma_{e,ion}$ can be changing during the operation of an IG, which will directly affect the precision and the stability of the pressure measurement.
2. Electron stimulated desorption (ESD) from the anode grid, the second term in Eq. (1) (b in Fig. 10). If the anode is covered with impurities, typically adsorbed water, CO and organic species, electron bombardment will induce their desorption. When the desorbed species are slow ions, they will be attracted towards the collector. If the desorbed species are neutrals, they will enter the ionizing volume and eventually increase the gas pressure locally.
3. Electron induced secondary electron emission from the grid, the third term in Eq. (1) (c in Fig. 10). Electrons hitting the grid can also induce secondary electron emission. In addition, some electrons will be elastically backscattered from the grid surface. The backscattered and high energy secondary electrons will have enough energy to ionize the gas atoms.
4. Electron beam induced X-ray emission (d in Fig. 10), the fourth term in Eq. (1). Electron bombardment of the grid affects the soft X-ray emission due to the bremsstrahlung effect or due to the excitation/deexcitation of grid atoms. X-ray photons may hit the collector and produce secondary electrons which will then be measured as the collector current. In the inverse X-ray effect (e in Fig. 10) X-ray photons hit the grounded shield of the gauge and the produced photoelectrons can drift to the collector which is also on ground potential.

In addition, there are outgassing and pumping effects which are also related to surface effects. The warming by the hot cathode causes additional desorption and outgassing of the electrodes and the surfaces cleaned by electron bombardment may readsorb molecules.

In the following, we shall review the literature related to the introduced surface effects in the above order, except for X-ray limit, which was already discussed in section 2.2.

5.1. Ion induced secondary electron yield from the collector (IISEY)

As stated before, secondary electrons contribute to an increase of the positive current measured on the collector. If the secondary yield changes in time, then the pressure reading will also change in the same proportion. This yield and its change depend much on the chosen material and on its surface composition. In the literature we can find many works useful to understand this process. Ion induced secondary electron emission ($\gamma_{e,ion}$ in Eq. (1)) is either induced by the *kinetic* or the *potential* energy of the ionic projectiles.

The *kinetic* electron emission, dominant at high projectile energies (ions of several keV to MeV region), is much more studied in the literature. In HCIGs with low energy projectiles the potential electron emission is expected to play the main role.

It is usually considered that the kinetic electron emission is caused by the momentum transfer from the ion to the electrons [93]. By accepting the simple approximation that the valence electrons in a metal are free and that the electrons at the bottom of the valence band have zero kinetic energy, one can define the threshold for the kinetic energy E_{th} of projectiles with mass M that are able to provide kinetic electron emission [94]:

$$\frac{E_{th}}{M} = \frac{1}{2m_e}\cdot\left[E_F - \sqrt{E_F\cdot(E_F+\phi)} + \frac{\phi}{2}\right] \tag{3}$$

where E_F is the Fermi energy measured with respect to the bottom of the valence band, ϕ the work function, and m_e is the electron mass. In the case of Al ($E_F = 10.6$ eV, $\phi = 4.3$ eV) the ratio E_{th}/M is 170 eV/u [95], whilst in the case of gold it would be 270 eV/u when the appropriate effective electron mass is applied in the upper formula [96]. Clearly, in the energy range of interest (up to 300 eV) a significant contribution of the kinetic electron emission can be expected only in the case of H^+ projectiles.

The main characteristic of the *potential* electron emission is that its probability is practically independent on the ionic projectile kinetic energy. The first relevant model of the potential electron emission was introduced by Hagstrum [97–100]. When approaching the metal surface, ions can be neutralized in two main non-radiative processes, Auger neutralization and resonant neutralization followed by Auger deexcitation. These processes are illustrated in Fig. 11.

Typical example of Auger neutralization process is interaction of slow He^+ ions, which have high ionisation potential E_I, with metals (Fig. 11 (a)): one electron from the valence band is occupying the empty valence state of the ion, followed by Auger electron emission from the valence band. This is the dominant neutralization mechanism for most of the ion-surface systems. Alternatively, if there is an unoccupied ionic level lying in-between the bottom of the valence band and the Fermi level of the metal, an electron from the valence band will tunnel onto the empty ion level (resonant neutralization, Fig. 11 (b)), thus forming an excited neutral projectile. Auger deexcitation of the neutral projectile will then take place by (2a) electron transfer from the valence band to the empty valence level of the projectile followed by the electron emission from the excited projectile state or, (2b) by the electron transfer from the excited to the valence projectile level followed by the electron emission from the valence band (Fig. 11b). This scenario is characteristic for Ne^+ ions.

The main condition for the performance of Auger neutralization and the corresponding electron emission is that $E_I \geq 2\phi$. It is also clear from Fig. 11a that the part of the valence band from which electrons can be emitted in an Auger process is increasing with the ionisation potential. The size of this part will determine the yield of emitted electrons. In addition, increase of the ionisation potential increases the energy of the emitted electrons and, consequently, the probability of their transmission over the surface potential barrier. Based on the simple assumptions introduced by Hagstrum in his original model [98], Kishinevsky formulated the following relation between the ion induced secondary electron yield $\gamma_{e,ion}$ [101]:

$$\gamma_{e,ion} = \alpha\cdot(\beta\cdot E_I - 2\phi) \tag{4}$$

Kishinevsky calculated that the parameters α and β should be $0.2/E_F$ and 0.8, respectively. On the other hand, Baragiola and co-workers fitted a set of different experimental results obtained on various systems to the expression (4), and obtained very good agreement for $\alpha = 0.032/E_f$ and

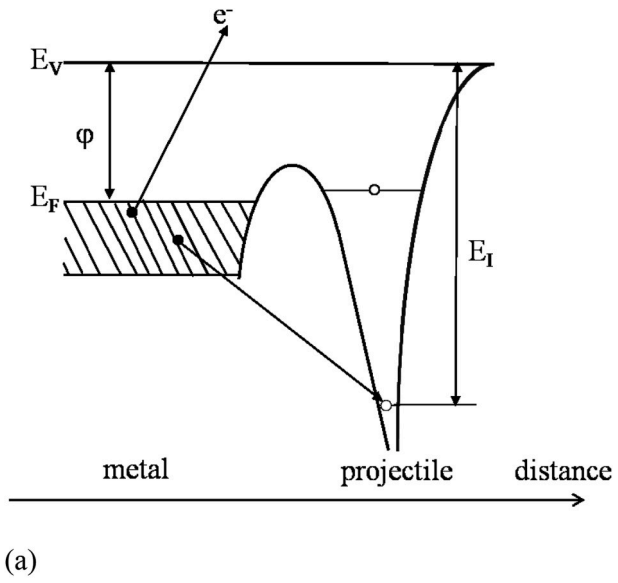

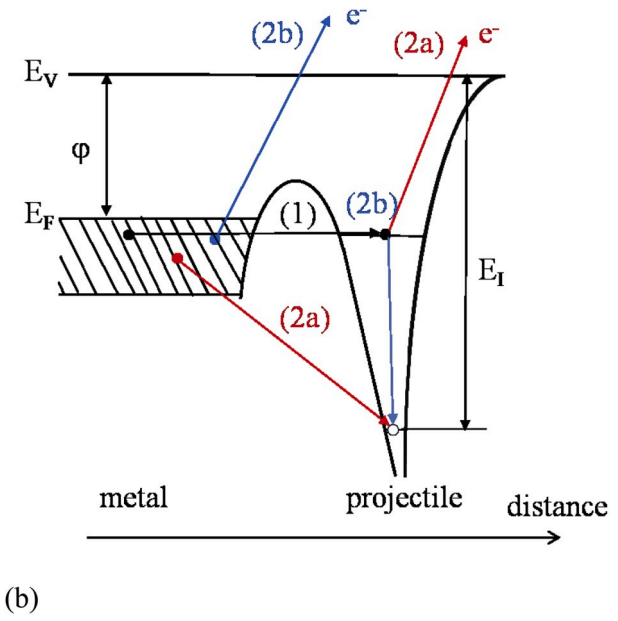

Fig. 11. (a) Schematic of the Auger neutralization process of a slow ion approaching surface of a metal yielding in an electron potential emission. E_V is the vacuum level i.e. potential energy of electrons far from the projectile and the surface. E_I is ionisation potential of the projectile.
(b) Schematic of the two-stage neutralization of an ion approaching surface of a metal: (1) resonant neutralization and occupying excited projectile state is followed by (2) Auger deexcitation in which an electron is emitted. Auger deexcitation may take place via two independent branches.

$\beta = 0.78$ [102].

Contrary to the expectations, it was observed that for some systems, $\gamma_{e,ion}$ was energy dependent well below the threshold for the kinetic energy emission (cf. eq. (3)). Typical examples are interaction of Ar atoms and ions with contaminated metallic surfaces [103] as shown in Fig. 12. Although the proximity of the ion to the surface affects the ionisation, such a significant relative change of γ_i cannot be explained by the potential electron emission. This phenomenon is being also observed for neutral atoms, which is a definite proof that the responsible effect is some kind of sub-threshold kinetic electron emission. Later, it was proposed that this specific type of electron emission is originated from transiently formed autoionizing quasi-molecules [104,105]. This effect

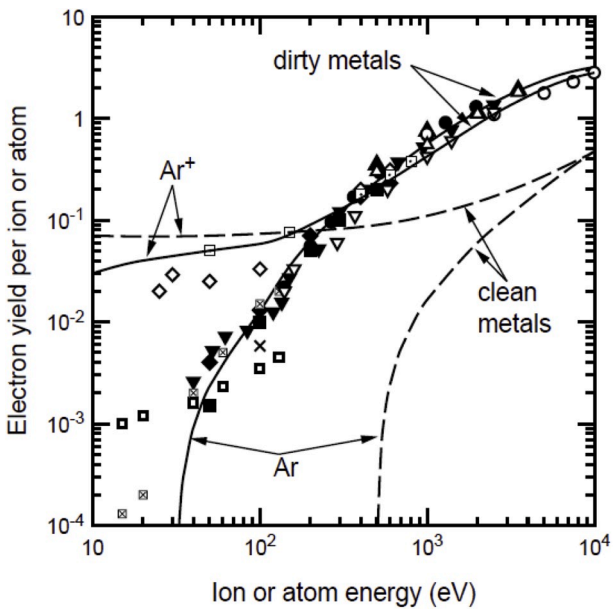

Fig. 12. Energy dependence of secondary electron yield induced by Ar ions and neutrals from different dirty metals [103]: □, Pt; ○,◇,◆ Cu; ▼,▽ Au; ⊠,▲,△ Ta; × , W; ■ CuBe; ● unknown; ▣, brass. Dashed lines are representative curves for clean metals. © IOP Publishing. Reproduced with permission. All rights reserved.

was initially observed and explained by Fano and Lichten, who developed electron promotion model for symmetric Ar–Ar collisions in gas phase [106]. The model was subsequently extended to asymmetric collisions by Barat and Lichten [107]. On the example of Ar^+ and Li^+ ion induced emission from clean aluminium, specific peaks in the energy spectra of emitted electrons were attributed to Auger transitions related to highly excited Al states [108]. It is worth noting that the electron promotion can take place due to both projectile-target atom and fast atom-atom collisions, since projectile will transfer part of its kinetic energy to target atoms during the surface interaction.

Influence of surface conditions of tungsten and platinum, as materials considered for ion collectors, on their work function was investigated in Ref. [109]. Long term operation of IGs improves their stability but reduces sensitivity. The investigations show that the typical contaminants in air exposed samples were mainly C and O (tungsten), and C, O, S, K, Ca and Ag (platinum), as detected by Auger Electron Spectroscopy. The samples were surface cleaned by annealing (tungsten at 1500–2000 °C, and platinum at 600–900 °C). Clean surfaces had work function increased for 0.7 eV in W) and for 0.6 eV in Pt. According to the Hagstrum theory, work function increase reduces IISEY (cf. eq. (4)), which explains reduction of the sensitivity.

Another design, screened IG was proposed by Gentsch and co-authors [76], in the form of a nearly closed system with all electrodes covered by gold. The screened IG provides well defined ionisation path lengths and clean electrode surface (whilst operating at 250 °C). The latter secure stable work function of the collector, which provides stable IISEY. The authors state that tempered and Ar sputtered gold surfaces provide reasonably stable work functions, which secure collector current stability. Closed construction increased X-ray induced photoelectron current from the collector. Two different supported materials were used – Pt–Ir, and W. It appears that Au coated tungsten has better properties due to the absence of solubility of gold in tungsten.

IISEY of 140 eV ions were measured for different ion-material combinations (Ar, N, CO, H, and Au, C) [110]. It was shown that IISEY strongly depends on both the ion species and the material, spanning from 2 to 12%.

Sensitivity variations of BAGs due to the collector contamination by

different gases were studied in Ref. [111]. Different collectors (flash heated W, sputter cleaned W, sputter cleaned carburized-W, and flashed Pt-clad Mo) and different contamination gases (N_2, CO, O_2, H_2) were combined. The test gases were Ne, He, Ar. In the experiments, there were a reference and a test BAG. The test BAG was exposed to the contamination gases (10 min at 10^{-7} Torr) and the pressure reading with before and after the contamination was compared with that of the reference BAG. Tungsten collectors, both flash heated and sputter cleaned showed changes in sensitivity up to 10% for different gases, most for CO, O_2 and H_2. Pt-clad Mo and carburized W were changing sensitivity up to ±3%. Since the latter is fragile and harder to handle, it was concluded that Pt-clad Mo is the best option for the collector.

A less discussed effect is the change of work function by ion bombardment. In Ref. [112] the authors studied the effect of bombardment of 100–600 eV noble gas ions and the post-bombardment annealing on the work function change of W and Au. For Ar^+ ion fluence of $1.6{\cdot}10^{15}$ cm^{-2}, the work function of W increases with the energy. In the case of He^+, the work function increase seems to be independent on the ion energy for the fluence fixed at $3.8{\cdot}10^{15}$ cm^{-2}. In both cases, the work function change increases with the ion fluence. Its change is of the order of few tenths of eV. The post-bombardment annealing lead to the work function recovery for the temperatures of about 800–1000 K or greater. Contrary to tungsten, ion bombardment of Au reduces the work function. The trends with the ion energy and fluence were not well defined in contrast to tungsten, but the typical work function reduction appears to be about 0.2 eV. Although explanations were not provided these findings may be related with change in the surface composition or the surface morphology [113].

5.2. Electron stimulated desorption

In many HCIGs electron trajectories typically end on the grid with energy above 100 eV producing desorption of neutrals and eventually of ions, generating the described extra contribution to the pressure reading. There are plenty of different models used for the description of Electron Stimulated Desorption (ESD) of both neutrals and ions [114]. Here, we review two models of potential significance in HCIGs.

One of the earliest, and still very popular and relevant, models was introduced independently by Menzel and Gomer [115], and Redhead [116] (MGR model). In this model it is assumed that the chemically adsorbed species (A) and the metallic surface (M) are initially in the ground-state configuration and its excitation by electrons is treated in the frame of the adiabatic semi-classical approximation. The bombarding electrons can excite the system into different states, such as antibonding, or A^+–M^- state. When the system is excited in the antibonding state electron excitation will contribute to the repulsion of the adsorbate and its acceleration. In the case of the ionisation the same effect will take place due to the Franck-Condon principle. If the system stays long enough in an excited state, the adsorbate will be repelled from the surface and therefore gain enough kinetic energy to overcome the energy barrier once it returns to the ground state. Alternatively, in the case of the ionized excitation state, the adsorbate may leave the surface as ion. The latter process is not highly probable: it is much more likely that Auger neutralization will take place, according to the Hagstrum model [98].

Information on the adsorption sites and the character of the adsorption can be revealed from the energy analysis of desorbed ions. The technique is known as ESD Ion Energy Distribution (ESDIED). In addition, particularly interesting features were obtained from the angular distribution of ESD ions (ESDIAD) [118].

An investigation of oxygen adsorption on tungsten by ESDIED has been performed in Ref. [119] identifying three different sites with adsorption energies from 3 eV to 8 eV.

In [120] the authors measured energy distribution of hydrogen and deuterium ions produced by ESD from a platinum grid. By monitoring time evolution of energy and mass selected signals, three different chemisorption sites of H_2 were identified, some of which are not dissociative.

Influence of the ESD ions on the pressure measurement from the Mo grid on which oxygen was adsorbed were investigated by Redhead [116,121,122]. The result of ESD is desorption of atomic oxygen, both neutrals and ions. The ionisation efficiency of neutral atomic oxygen (formation of O^+) has a threshold at about 17.6 eV of electron energy and reaches maximum at about 100 eV. It appeared that the fraction of directly emitted ions, mainly O^+, from the grid in the ESD process is about 2% of the total collected ions in the electron energy range from (60–200) eV. The initial energy of desorbed ions is typically around 6 eV, so it will always reach about the same value whenever ions re-approach the grid. Consequently, the ions have enough energy to overcome this potential barrier and leave the ionisation volume. When that happens, electric field established between the grid and the envelope will accelerate them away from the BAG. In other words, these ions can leave the volume of the BAG without being collected.

In [121] a list of references is given for studies in which ESD on different contaminated materials were investigated (mainly from the 1960s). By summarizing these results, Redhead indicates that gauge exposure of O_2 or CO on W leads to the emission of O^+. Mo, W and Pt–Ir show similar behaviour in terms of ESD, whilst Pt-clad Mo seems to have better properties and should be preferable as the grid material. We stress that this conclusion is in contrast with the more recent work of Watanabe [123,124], who preferred pure Pt or an alloy of 80% Pt −20% Ir. However, Watanabe was using special procedures for the grid cleaning.

The highest ion yields (those of O^+) are expected from metallic oxides having the highest valence (TiO_2, Ta_2O_5, WO_3 and Nb_2O_5) [87]. This type of ESD was firstly observed and explained by Knotek and Fiebelman [117].

Together with the X-ray limit, ESD and outgassing represent lower limits for pressure measurements. The latter two processes are correlated since electron bombardment of the grid also causes heating [125]. Three different grid materials were studied: Pt-clad Mo, W(74%)-Re (26%) alloy and gold-plated stainless steel. Both processes (ESD and outgassing) are dominated by hydrogen emission in the considered pressure range. The Pt-clad Mo grid showed an ESD reduction with the grid temperature, but outgassing began to dominate above 600 °C. The W–Re alloy grid showed a large thermally activated ESD effect. The Au-plated stainless-steel grid showed the smallest ESD effect, but with the largest outgassing.

Behaviour of the ESD contribution to the ion current as a function of subsequent introduction and pumping of different gases was studied in Refs. [123,126–128] using the ion spectroscopy gauge. Gas introduction/pumping cycles of H_2 and H_2O yielded in hysteresis loops of the ESD ion signal. In the case of water vapour, the hysteresis effect was particularly pronounced after both bake-out and electron bombardment, suggesting that the Pt–Ir anode surface worked as a catalyst in the production of ESD ions. Experiments with hydrogen revealed that the hysteresis loop was the most pronounced after electron bombardment of non-baked grid, whilst after baking no hysteresis was observed.

5.3. Electron induced secondary electron emission

Some high energy electrons are also produced when the electrons from the cathode end their trajectory on the grid. These electrons may have enough energy to further ionize the gas particles. Again, changes in their yield lead to changes in the pressure reading.

The spectrum of electrons emitted from a surface irradiated by primary electrons of energy E_0 is usually divided in three regions [129]:

- electrons with energy below 50 eV, usually called true secondary electrons;
- electrons with energy equal to that of the primary electrons E_0 are elastically backscattered;

- electrons with energies above 50 eV but below E_0 are considered as inelastically backscattered electrons.

The main quantities of practical interest related to this phenomenon are total and secondary electron yield (TEY and SEY), respectively defined as the mean numbers of all or true secondary electrons per incident primary electron. In the case of metals, maximum SEY is usually in the range 0.8–2, depending on the surface conditions (purity, surface morphology), and it is obtained for E_0 in the range (200–400) eV.

Electron induced secondary electron emission is considered as a three-step process:

a) incident electrons penetrate into the bulk material and lose their energy by exciting the electrons in the sample, which may have enough energy to be emitted (internal secondary electrons);
b) internal secondary electrons move through the material, collide with atoms and electrons and lose their energy in this process;
c) electrons that reach the surface and have energy above the vacuum level encounter refraction of their trajectories on the interface and become emitted to vacuum with some probability.

In the energy range of interest for ionisation gauges, the most efficient electron energy loss mechanism is excitation of valence electrons (direct, or via plasmon formation followed by Landau damping) [130]. SEY of dielectrics is much higher than that of clean pure metals due to the low energy loss probability of internal secondary electrons.

Baglin and co-authors illustrated that SEY of technical surfaces are significantly higher than that of well-prepared material samples i.e. sputter cleaned and/or vacuum annealed [131]. They also summarized three general approaches used to decrease SEY of different materials: surface coating by a material having low and stable SEY, increasing the surface roughness, and intense electron bombardment in order to promote growth of carbon-based overlayer with low SEY.

Werner and Leck observed on a set of BAGs the change of sensitivity for hydrogen depending on the filament temperature [132]. Closer inspection showed that the effect is related to the surface conditions of the grid. Since it is known that atomic H can be formed on tungsten surface at temperatures above 1900 K, the proposed explanation is that higher temperature filaments produce more atomic hydrogen which is later adsorbed on the grid surface. The authors further argue that the presence of hydrogen at the grid surface increases the number of backscattered electrons with enough energy to contribute to gas ionisation.

The SEY induced by 100 eV electrons, was measured in the case of Mo, C and Au [110]. The estimated fraction of secondary electrons having energy above 20 eV, which can contribute to further ionisation is in the range 10–20%, depending on the sample cleanliness and the material.

Total and partial electron yield induced by the 100 eV primary electrons were measured in Ref. [133] from polycrystalline Mo, gold plated W foil and Mo covered with graphite spray. While the total electron yield is of the order of unity, the partial yields for $E > 20$ eV, $E > 30$ eV and $E > 40$ eV were typically ~0.2, ~0.15 and ~0.09, respectively. When comparing different materials, electron emission from carbon surface may be slightly lower than from the other two surfaces (~0.15 for $E > 20$ eV). The authors estimate that the secondary electrons typically contribute to the 10% of the total sensitivity of an HCIG.

5.4. Other surface effects

Any effect that may change the gas concentration or the measured ion current is relevant for the gauge stability. Smith et al. investigated the process of hydrogen interaction with hot filament in Ref. [134]. The emitted atomic hydrogen atoms can be trapped in the chamber walls causing a pumping effect. In Smith's work, the probability of H formation was measured: the threshold for the dissociation is at about 1900 K, whilst the plateau of the probability equal to 0.3 is reached at about 2500 K–3000 K probably related to the oxygen contamination of the tungsten surface.

The process of hydrogen adsorption on polycrystalline rhenium was studied in Ref. [135], Hirsch [136] investigated the surface ionisation on the hot tungsten filament.

Another surface effect that might have a role is surely the problem of X-ray limit. The coefficient of X-ray emission induced by electrons is strongly Z-dependent (Z: atomic number) and it would be favourable to work with low Z materials.

5.5. Outgassing and pumping effects including chemical reactions of molecules on hot filament

According to Redhead [58], the total pumping speed of an ionisation gauge is composed of two components: electronic and chemical pumping speed. Redhead names "electronic pumping" the removal of positive ions by ion implantation into the ion collector and the envelope. The chemical pumping is a result of chemisorption of gas on the electrodes and on any evaporated or sputtered films. Chemical pumping may also occur when highly reactive molecular fractions, which are produced by electron impact, chemically interact with other molecules on the surfaces and adsorb.

It is worth noting that Redhead [58] found a pumping speed of 2 l/s for nitrogen in a BAG operated at 8 mA electron current and 250 eV electron energy when the gauge was first operated. It reduced to 0.25 l/s, after 10^{17} molecules had been pumped.

A comprehensive review of methods of pumping speed and outgassing measurement and summary of published results is given in a paper of Berman [137]. Pumping speed in the range from 10^{-3} l/s to 0.5 l/s were reported for various gases and gauge conditions.

The tungsten filament of an ionisation gauge is operated at temperatures near 2000 K. At this temperature H_2, O_2, H_2O and some hydrocarbons are thermally dissociated [58]. Reactions between atomic hydrogen and carbon impurities in the tungsten filament produce CH_4. Reactions of atomic hydrogen with oxygen from the oxide surface layer of the metallic parts produces H_2O, and reaction of oxygen with carbon impurities from filament produce CO and CO_2 [58,138,139].

Moraw [139] compared pumping speed and outgassing rate of two nominally identical Bayard-Alpert gauges with different filaments installed: tungsten and thoriated iridium. Both gauges were operated at 100 μA. Pumping speed as high as 1.5 l/s was measured for O_2 onto a tungsten filament, while for thoriated iridium it was 0.5 l/s. For H_2 and tungsten filament the pumping speed was 0.28 l/s, while for thoriated iridium it was 0.14 l/s. Moraw measured the outgassing rate of gauges during operation, after a 20 h bakeout at 100 °C. In addition, he also measured with a quadrupole mass spectrometer changes of the residual gas composition in his vacuum system when filaments were switched on and off. In the case of BAG with tungsten filament the total outgassing rate was $1.5 \cdot 10^{-8}$ mbar l/s (N_2-equivalent), and the dominating gas species was CO (64%). In the case of thoriated iridium the total outgassing rate was $2.7 \cdot 10^{-8}$ mbar l/s with H_2 as dominating species (50%). Despite higher operating temperature, the gauge with tungsten filament had lower net N_2-quivalent outgassing rate due to higher pumping speed for hydrogen, which was a consequence of much more effective dissociation at higher temperature.

6. Sensitivity and stability

Sensitivity S is expressed by (ISO 27894) as

$$S = \frac{I_c - I_0}{I_e (p - p_0)} \tag{5}$$

where I_c is the collector current at pressure p, I_e the electron emission current in the filament, I_0 the collector current at the base pressure p_0.

The relative sensitivity factor (ISO 27894) for a gas species X is given by:

$$r_X = \frac{S_X}{S_{N_2}} \tag{6}$$

with S_x the gauge sensitivity for the gas X.

The ratio r_x is a key parameter in vacuum processes where other gases than nitrogen are used.

6.1. Relative sensitivity factor

Nakao [140] describes experiments where ionisation gauge sensitivities relative to nitrogen were determined using the ionisation cross section for inorganic and hydrocarbon gases. The experimental results, made for electron energy of 75 eV, are presented in Fig. 13. Knowing the gauge sensitivity for nitrogen, the sensitivity for other gases can be estimated from the empirical results. Uncertainties, however, associated to sensitivities and ionisation cross-section measurements are relatively high (up to tens of percent). It is evident that the ionisation cross-section (near 100 eV) is the most suitable parameter to predict the relative gauge sensitivity [141]. Because ionisation cross section is linearly related to molecular polarizability [142], relative gas sensitivity factors can also be related to polarizability [143].

Labrune et al. [71] proposed an apparatus to measure the total ionisation cross sections based on a molecular collision method. The authors compared gauge coefficients determined from the measurements and specification data of a commercially available ionisation gauge. They claimed a relative discrepancy of less than 8%.

A large number of relative sensitivity factors are reviewed in a technical note from the NASA in 1969 [144]. The report also tests several empirical relationships of r_x with ionisation cross section, polarizability, number of electrons in the molecule, refractive index and other quantities. The variation from gauge to gauge is typically 7%, the uncertainty of the relative sensitivity prediction from peak ionisation cross section is 10%–15%.

Flaim also reviewed in 1971 [145] relative sensitivity factors for common gases, such as H_2, He, Ne, N_2, Ar, CO, CO_2, H_2O, O_2, Kr, Xe, Hg, Cd. This study pointed out some scatter in the values for Ar, CO_2 or O_2.

Seven commercial 'broad range' ionisation gauge tubes were experimentally studied by Tilford [147] in 1982 for N_2, Ar, H_2, D_2 and H_2 between $1{\cdot}10^{-4}$ and 0.1 Pa.

In 1991, Filipelli [146] made sensitivity measurements in a large pressure range ($5{\cdot}10^{-8}$ to $1{\cdot}10^{-3}$ Pa) for 16 ionisation gauges, extractor type or Bayard-Alpert type, and 3 gases: He, N_2 and H_2.

The study of Jousten in 1995 [148] determined different gauge sensitivities to H_2 and D_2 which is interesting, since the ionisation probabilities are the same. 12 different gauges, Bayard-Alpert or extractor types were investigated and significant differences for the two gases were found.

Li and Jousten [149] analysed the relative sensitivities of three models of stable commercial ionisation gauges, namely IE414 (BAG) and IE514 (extractor gauge) from Leybold and Stabil Ion from Granville Phillips (BAG) for Ar, He and H_2. The two BAGs exhibited similar relative sensitivities.

Yoshida and Arai [150] measured relative sensitivity factors of a BAG and an extractor gauge for 24 gas species including inert gases, hydrocarbons, oxygen, carbon oxide, chlorofluorocarbons, and liquid vapours. They compared their own results with data from other authors and found a significant spread of the r_x values for some gases like e.g. helium (r_{He}: 0.14 … 0.20), neon (r_{Ne}: 0.22 … 0.36), argon (r_{Ar}: 0.9 … 1.4) or propane (r_{C3H8}: 2.92 … 4.55).

6.2. Time stability of ionisation gauges

By time stability, distinction can be made between short and long-term stability.

Short-term stability is based on the stability over several hours up to a few weeks [149]. The maximum deviations over 72 h (at 10^{-4} Pa) were determined to be within a few tenths of a percentage, but 2%–5%, if a period of 6 months was considered.

NIST analysed a wide panel of gauges, mainly from customers' calibrations [151–153]. In Ref. [151] the stability of 4 ionisation gauges was investigated over 500 days; the gauges were triode-type or Bayard-Alpert-type, all with tungsten filament. In Ref. [152], the authors collected calibration data in N_2 from 20 gauges customers on a period of 10 years, and sorted them in a database. Then they could study different characteristics such as the stability of the correction factor of the gauge with its electronics box. Gauges with tungsten filaments showed a higher stability than those with ThO_2–Ir filaments. An uncertainty denoted long-term uncertainty was estimated from successive calibrations (with a periodicity of more than one year). This uncertainty ($k = 1$) lied between 1.9% for gauges operated at 4 mA and 2.8% for those operated at 0.1 mA.

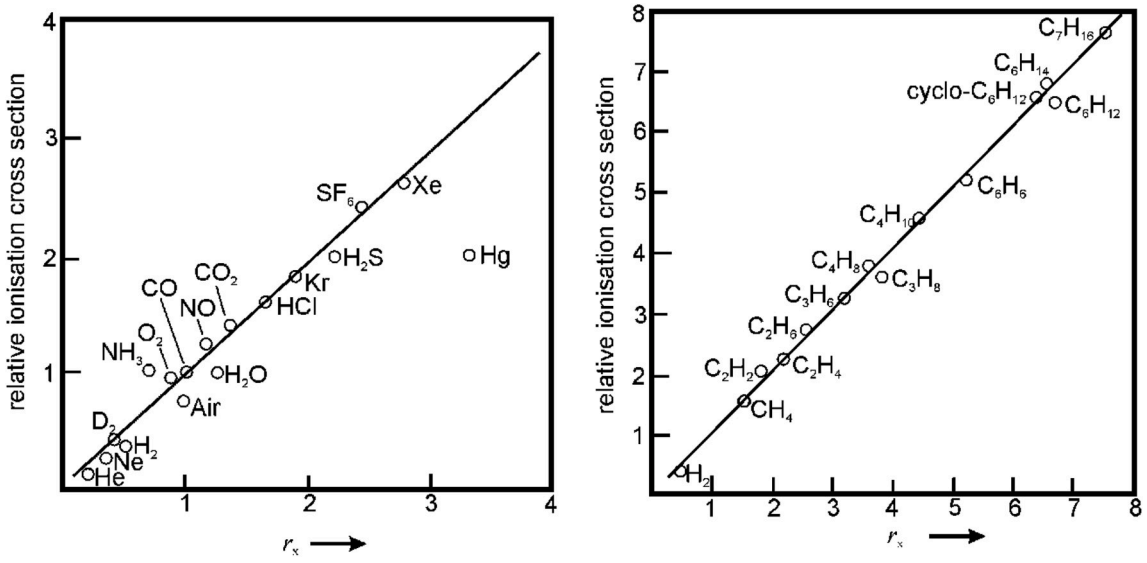

Fig. 13. Relationship between the gauge sensitivity relative to nitrogen (r_x) and the ionisation cross-section relative to nitrogen for inorganic molecules (left side) and organic molecules (right side). Redrawn from Ref. [140].

Other stability results were published by Poulter [154,155], Warshawsky [156], Arnold [32] and Yoshida et al. [157–159]. Poulter [154] measured a decrease of sensitivity of a triode gauge of 6% within 6 months, after which it became more stable. In Ref. [155] triode gauges were found to be significantly more stable than BAGs, especially after intermediate exposure to atmospheric pressure. Yoshida et al. [157] found that the sensitivity of four ionisation gauges decreased by 2.6%–5.4% during a period of 1 year, for an extractor and axial-symmetric transmission gauge [158] they found a long-term stability within 3% in a period of 7 months, in a period of 3 years the changes of sensitivity ranged up to 13% [159].

6.3. Linearity

Few papers only deal with the change of gauge sensitivity as a function of pressure. Filippelli [146] concluded that for N_2 and He, in the pressure range from $5{\cdot}10^{-8}$ to $1{\cdot}10^{-3}$ Pa ionisation gauges were linear within ±4%. The same conclusion was made for H_2 in the range $1{\cdot}10^{-7}$ to $1{\cdot}10^{-4}$ Pa. His work was based on 16 commercial gauges.

In [149] such results are provided for relative sensitivities, between 10^{-6} and 10^{-3} Pa, for Ar, He and H_2. Graphs indicate that the gauge linearity for the above-mentioned gases is similar to that obtained with N_2 within about 1%.

During an international comparison when a BAG and a extractor gauge were transported between continents, it was found that an extractor gauge, originally nonlinear by 6%, got a linear characteristic after transport [160]. Yoshida et al. [158] found for an extractor and axial-symmetric transmission gauge non-linearities < 3% down to a pressure of 10^{-9} Pa for hydrogen, nitrogen, and argon. Also, Li [161] found a non-linearity of only 2% of an extractor gauge from $4{\cdot}10^{-10}$ Pa to $1{\cdot}10^{-3}$ Pa.

6.4. Temperature dependence of sensitivity

The ambient temperature influence was studied in detail in Ref. [162]. The authors linked the temperature coefficient partly to the thermal transpiration influence and estimated it to be about $-0.3\%{\cdot}K^{-1}$.

6.5. Operating parameters and procedures influence

Ionisation gauge sensitivity may vary significantly upon the way of using it, which includes operating electrical parameters and operating procedures.

In [148] the sensitivity ratio of H_2 to D_2 was analysed after several procedures: gauge venting and degassing, ion bombardment with Ar, suppressor or grid potential.

Tilford [163] provided some guidance for conditioning and using a Bayard Alpert gauge when making measurements to keep it stable over time:

- avoid high pressure (over 1 Pa) exposition,
- operate the gauge with an emission current of 1 mA or less,
- ensure to maintain bias voltage within a few volts and emission current within a few percent,
- keep the gauge clean.

For the latter, the ionisation gauge must be degassed and/or baked out *i.e.* impurities on the surface of the materials are ejected with the rise in the gauge temperature.

Watanabe, however, recommended a higher emission current than 1 mA ([125]) to have a steady high electron flux onto the grid in order to reduce adsorption of molecules onto the grid and reduce ESD of neutrals and ions.

7. Numerical simulations

The first step in simulations is to calculate the electrical potential distribution generated by the biased electrodes inside the gauge. The second step is to calculate the electron and ion trajectories once the initial conditions are given. Inclusion of space charge effects and secondary electrons from gas phase and/or surfaces greatly improve the significance of the simulation. On the top, also the simulation of X-rays within the gauge may be included.

There are several numerical methods available. Today, with the advent of powerful computers, three methods are used most often:

Finite difference Method (FDM), Finite element method (FEM) and Boundary element Method (BEM).

An overview of these methods can be found in McFadden and Wüest [164] and references therein.

A popular electrostatic FDM package is SIMION [165,166]. ANSYS and COMSOL Multiphysics are popular FEM packages that have add-on packages for electromagnetic field calculation and particle ray tracing.

In the literature there are found only a few papers on numerical simulation of HCIGs [21,24,25,167–173].

Turner and Priestland [170] used a custom code written in the computer language Algol to investigate the sensitivity differences between Bayard-Alpert gauge with and without closed anode cage. Kudzia and Slowko [171] used a probabilistic method to simulate ionisation characteristics in a plane symmetric electrode system, plane asymmetric electrode system and a system with a spherical electrode anode. Pittaway [174] used CAD techniques to study the influence of electrode spacing and potentials on the path length of electrons. Kauert et al. [167] investigated hot cathode ionisation gauges with a custom three-dimensional numerical calculation program IONTRA3d, after having concluded that SIMION 4.0 2.5D was not suitable for their needs. IONTRA3d is also a FDM code. They conclude that anode support sticks play an important role in the special shape of the sensitivity-cathode voltage plots. Schopphoff [172] simulated an extractor gauge with SIMION.

Bills et al. [21] used SIMION to simulate a Bayard-Alpert gauge and from the insight gained into the causes of nonstable behaviour of Bayard-Alpert gauges developed the Stabil Ion Gauge.

Juda et al. [169] simulated a CERN-type modulated Bayard-Alpert gauge and a Helmer gauge with the 3D-simulation software Vector Fields OPERA 3D and found very good agreement of calculated and measured sensitivity. Recently, Silva et al. [173] used SIMION 8.1 to study the electron path distribution, the ion collector efficiency and the contribution of backscattered electrons for the ionisation of the BAG design investigated in Ref. [169].

8. Conclusions

It is evident from the literature review that very few publications exist dealing with the optimization of the geometry of the HCIG to make it robust in terms of metrological stability, i.e. long-term stability of the sensitivity or calibration factor. The focus of developments was mainly on the extension to lower pressures starting in the 1960s until the 1990s. Also the physical effects within the gauges were no more discussed in this century, with the one exception by Peacock [27] in 2002, who discussed the importance of electron path length on the stability of Bayard-Alpert ionisation gauge. All other papers were published before 2000, which indicates that practically all present knowledge was matured in the 20th century. The most recent systematic study of various physical effects that influence accuracy of measurements with ionisation vacuum gauges (both hot cathode and cold-cathode) was published by Kendall [90].

From the literature we conclude that the following effects inhibit an improvement of the metrological characteristics of a HCIG, in particular the most widespread BAG:

1. The instability of the electron emission distribution from the cathode.

A changing distribution causes different electron paths and lengths and a changing sensitivity. Changing emission distribution is caused by changing cathode temperatures and potentials, work function, and ion bombardment. Included here is the geometrical variation and instability of the cathode in most of today's commercial gauges.

2. Secondary electrons produced on the collector by ion impingement.

The secondary electron yield on the collector will depend on its surface which is changing with time.

3. Space charge effects.

Positive space charge around the collector, in particular at higher pressure, perturbs the field distribution and affect ion and electron trajectories. The space charge depends on the type of ions and the number of secondary electrons and is usually not stable.

4. Electron stimulated desorption of neutrals and ions from the anode.

The number of desorbed ions and molecules changes with time due to the changing surface and can make a significant contribution to the ion current compared to gas phase ions.

5. X-rays produced by electrons impinging on the anode.

The X-rays generate numerous electrons within the gauge which cannot be controlled and will change the measured ion current in numerous ways.

The effects described in the publications make it rather improbable that a BAG design can ever lead to a vacuum gauge with satisfying stability for metrological and scientific needs. For this reason, for the purpose of a more metrologically stable ionisation gauge, we will pursue a design which is different from today's commercial HCIGs, mainly BAGs. We found the approaches of Bills et al. [23] and Klopfer [29] most interesting in this respect. These designs offer both the possibility of a well-defined electron path and the possibility to separate at least some of the surface effects from volume effects. The Klopfer design also offers the possibility to use a kind of point emitter of electrons avoiding the problem of locally changing electron emission. We also think that the Klopfer design opens the possibility for a better mechanical stability than with present HCIG which is important for metrological stability.

It is also clear that a highly accurate ionisation gauge will need an accurate emission current control and accurate ion current measurement over many decades. Emission control is preferred, because it is impractical for regular use to measure the electron current and use the calibrated sensitivity to determine pressure. It may be an option, if this can be done by digital processing. In our design, which will be published soon, the electron current and so the ion current will be much lower than in today's commercial gauges and challenge the effort and price of the electrical unit.

It was also a surprise that there were very few systematic investigations to use simulations to improve or design gauges. Instead, researchers in the academic or industrial field mostly used the trial and error method with devices. A good example is the work of Watanabe who based the improvement of the next generation gauge on the experience with the former generation. It can be concluded that the employment of simulations, as is being done by our consortium, can lead to a significant step of an improved gauge design.

Declaration of competing interest

The authors declare that they have no known competing financial interests or personal relationships that could have appeared to influence the work reported in this paper.

Acknowledgements

This work has received funding from the EMPIR programme (project 16NRM05 'Ion gauge') co-financed by the Participating States and from the European Union's Horizon 2020 research and innovation programme.

References

[1] ISO 27894:2009.
[2] O. Von Baeyer, Phys. Z. 10 (1909) 169.
[3] O.E. Buckley, An ionization manometer, Proc. Natl. Acad. Sci. U.S.A. 2 (1916) 683.
[4] R.T. Bayard, D. Alpert, Rev. Sci. Instrum. 21 (1950) 571.
[5] D. Li, K. Jousten, Comparison of the stability hot and cold cathode ionisation gauges, J. Vac. Sci. Technol. A 21 (2003) 937–946.
[6] K. Jousten, Total pressure vacuum gauges, in: K. Jousten (Ed.), Handbook of Vacuum Technology, second ed., Wiley-VCH, Weinheim, 2016 (chapter 13).7.
[7] F.A. Baker, J. Yarwood, Die Erzeugung und Messung von Ultrahochvakuum Teil 1, Vakuum-Technik 6 (7) (1957) 147–153.
[8] P.A. Redhead, E.V. Kornelsen, Neue Ergebnisse in der Ultra-Hochvakuum-Technik, Vakuum-Technik 10 (2) (1961) 31–39.
[9] H.J. Schütze, F. Stork, Über den Einfluß der Systemgeometrie und der Betriebsbedingungen auf die Gasionenkonstante von Ionisationsmanometerröhren nach Bayard-Alpert, Vakuum-Technik 11 (5) (1962) 133–141.
[10] J. Groszkowski, Collector dimensions and sensitivity in Bayard-Alpert ionisation gauge, Bull. Acad. Polon. Sci 13 (2) (1965) 15–22.
[11] J. Groszkowski, Bull. Acad. Polon. Sci 13 (1965) 3.
[12] J. Groszkowski, Bayard-Alpert ionisation gauge sensitivity vs. Collector position in anode cross section, Bull. Acad. Polon. Sci 13 (4) (1965) 57–59.
[13] J. Groszkowski, Bull. Acad. Polon. Sci 13 (1965) 261.
[14] J. Groszkowski, Bull. Acad. Polon. Sci 13 (1965) 397.
[15] J. Groszkowski, Bull. Acad. Polon. Sci 14 (1966) 1023.
[16] J. Groszkowski, Electrode dimensions of the Bayard-Alpert ionisation gauge and its sensitivity, Unknown J., 241–244..
[17] G. Comsa, Ion collection in the bayard-alpert gauge, J. Appl. Phys. 37 (2) (1966) 554–556.
[18] C. Benvenuti, M. Hauer, Low pressure limit of the bayard-alpert gauge, Nucl. Instrum. Methods 140 (1977) 453–460.
[19] H.C. Hseuh, C. Lanni, A thin collector Bayard-Alpert gauge for 10^{-12} Torr vacuum, J. Vac. Sci. Technol. (5) (Sep/Oct 1987) 3244–3246.
[20] R.N. Peacock, N.T. Peacock, Sensitivity variation of Bayard-Alpert gauges with and without closed grids from 10^{-4} to 1 Pa, J. Vac. Sci. Technol. A 8 (4) (1990) 3341–3344.
[21] P.A. Redhead, The sensitivity of bayard—alpert gauges, J. Vac. Sci. Technol. 6 (5) (1969) 848–854.
[22] W.B. Nottingham, Trans. AVS Vac. Symp. 8 (1961) 494.
[23] D.G. Bills, P.C. Arnold, S.L. Dodgen, C.B. Van Clev, New ionisation gauge geometries providing stable and reproducible sensitivities, J. Vac. Sci. Technol. A 2 (2) (1984) 163–167.
[24] D.G. Bills, Causes of nonstability and nonreproducibility in widely used Bayard-Alpert ionisation gauges, J. Vac. Sci. Technol. A 12 (2) (1994) 574–579.
[25] S. Suginuma, M. Hirata, Dependence of sensitivity coefficient of a nude-type Bayard-Alpert gauge on the diameter of an envelope, Vacuum 53 (1999) 177–180.
[26] A.R. Filippelli, Influence of envelope geometry on the sensitivity of ''nude'' ionisation gauges, J. Vac. Sci. Technol. 14 (1996) 2953.
[27] R.N. Peacock, Calibration stability of hot cathode ionisation gauges: a discussion of the importance of electron path length and gauge constant, J. Vac. Sci. Technol. A 20 (4) (2002) 1202–1203.
[28] K. Jousten, P. Röhl, Instability of the spatial electron current distribution in hot cathode ionisation gauges as sources of sensitivity changes, J. of Vac. Sci. and Technol. A 13 (4) (1995) 2266–2270.
[29] A. Klopfer, An ionisation gauge for measurement of Ultra-high vacua, in: Transact. Of the 8th Nat. Symp. of the AVS and 2nd Int. Congr, Pergamon, New York, 1962, p. 439.
[30] C.M. Sutton, K.F. Poulter, A new reference ionisation gauge for vacuum pressure measurement in the range 10-5 to 1 Pa, Vacuum 32 (5) (1982) 247–251.
[31] M. Hirata, M. Ono, H. Hojo, K. Nakayama, Calibration of secondary standard ionisation gauges, J. Vac. Sci. Technol. 20 (4) (1982) 1159–1161.
[32] P.C. Arnold, S.C. Borichevsky, Nonstable behavior of widely used ionization gauges, J. Vac. Sci. Technol. A 12 (1994) 568–573.
[33] P.C. Arnold, et al., Stable and reproducible Bayard-Alpert ionisation gauge, J. Vac. Sci. Technol. A 12 (2) (Mar/Apr 1994) 580–586.
[34] K. Schmidt, U. Bergner, Stabilität von Hochvakuum-Meßröhren, Vakuum in Forschung Und Praxis Nr 3 (1996) 178–181.

[35] S. Biehl, W. Knapp, C. Edelmann, Grundlagenuntersuchungen am Betriebsverhalten eines "Stabil Ion Gauge", Vakuum in Forschung und Praxis Nr 3 (1996) 189–193.
[36] P.A. Redhead, Ultrahigh vacuum pressure measurements: limiting processes, J. Vac. Sci. Technol. A 5 (5) (Sep/Oct 1987) 3215–3223.
[37] P.A. Redhead, UHV and XHV pressure measurements, Vacuum 44 (5–7) (1993) 559–564.
[38] P.A. Redhead, Modulation of Bayard-Alpert gauges, J. Vac. Sci. Technol. 4 (2) (1966) 57–62.
[39] F. Watanabe, Point collector ionization gauge with spherical grid for measuring pressures below 10^{-11} Pa, J. Vac. Sci. Technol. A 5 (2) (1987) 242–248.
[40] F. Watanabe, New X-ray limit measurements for extractor gauges, J. Vac. Sci. Technol. A 9 (5) (1991) 2744.
[41] J.C. Helmer, W.H. Hayward, Ion gauge for vacuum pressure measurements below $1x10^{-10}$ Torr, Rev. Sci. Instrum. 37 (1966) 1652–1654.
[42] C. Benvenuti, M. Hauer, Improved Helmer gauge for measuring pressures down to 10^{-12} Pa, in: 8th Int. Vacuum Congress, Cannes, 1980, pp. 199–202.
[43] L.G. Pittaway, The application of ion storage in electron space-charge fields to the design of a U.H.V. gauge and mass-spectrometer ion source Part II. The construction and performance of the extractor gauge, Philips Res. Rep. 29 (1974) 283–302.
[44] P.A. Redhead, New hot-filament ionisation gauge with low residual current, J. Vac. Sci. Technol. 3 (4) (1966) 173–180.
[45] P.A. Redhead, Measurement of residual currents in ionisation gauges and residual gas analyzers, J. Vac. Sci. Technol. Vol. A 10 (4) (1992) 2665–2673.
[46] F. Watanabe, Ion spectroscopy gauge: total pressure measurements down to 10^{-12} Pa with discrimination against electron-stimulated-desorption ions, J. Vac. Sci. Technol. A 10 (5) (1992) 3333–3339.
[47] F. Watanabe, S. Hiramatsu, H. Ishimaru, Using the modulating ion current for total pressure measurements below 10^{-10} Torr without errors caused by electron-stimulated ion desorption, J. Vac. Sci. Technol. A 2 (1) (1984) 54–56.
[48] H. Akimichi, N. Takahashi, T. Tanaka, K. Takeuchi, V. Tuzi, Improvement of the performance of the ionisation gauge with energy filter for the measurement of an extremely high vacuum, Vacuum 47 (6–8) (1996) 561–565.
[49] N. Takahashi, J. Yuyama, Y. Tuzi, H. Akimichi, I. Arakawa, Axial-symmetric transmission gauge: extension of its pressure measuring range and reduction of the electron stimulated desorption ion effect in ultrahigh vacuum, J. Vac. Sci. Technol. A 23 (2005) 554.
[50] B.R.F. Kendall, E. Drubetsky, Stable cancellation of X-ray errors in Bayard-Alpert gauges, J. Vac. Sci. Technol. A 16 (3) (1998) 1163–1168.
[51] A.R. Filippelli, Residual currents in several commercial ultrahigh vacuum Bayard-Alpert gauges, J. Vac. Sci. Technol. A 5 (5) (1987) 3234–3241.
[52] N.T. Peacock, Measurement of X-ray currents in Bayard-Alpert type gauges, J. Vac. Sci. Technol. A 10 (4) (1992) 2674–2678.
[53] T. Mitsui, T. Shigehara, Application of metal-insulator-metal thin films as cold cathodes to the Bayard-Alpert gauge, Vacuum 41 (7–9) (1990) 1802–1804.
[54] Handbook of Electron Tube and Vacuum Techniques by Fred Rosebury, AVS classics, 1964, ISBN 978-1-56396-121-2 reprinted 1993.
[55] Handbook of materials and techniques for vacuum devices by Walter H. Kohl, AVS classics, 1973, ISBN 978-1-56396-387-2 reprinted 1993.
[56] P.E. Gear, The choice of cathode material in a hot cathode ionisation gauge, Vacuum 26 (1) (1975) 3–10.
[57] R.O. Jenkins, A review of thermionic cathodes, Vacuum 19 (8) (1969) 353–359.
[58] P.A. Redhead, Errors in the measurement of pressure with ionisation gauges, in: Vac. Symp. Transactions AVS, C. R. Meissner, 1960, pp. 108–111.
[59] D. Alpert, Le Vide 17 (1962) 19.
[60] J. Gasperic, Die Regenerierung verunreinigter Wolfram-Kathoden von Ionisationsvakuummeter-Röhren, Vakuum-Technik 16, Jhrg. Heft 5 (1967) 109–110.
[61] B. Angerth, Z. Hulek, The tungsten evaporation limit of hot cathode ionisation gauges, J. Vac. Sci. Technol. 11 (1) (1974) 461–465.
[62] C. Edelmann, Zum Einfluß der Glühkatode auf den unteren Grenzdruck bei Bayard-Alpert Ionisationsvakuummetern, Exp. Techn. D. Phys. XXIII (1975) 525–532.
[63] P. Repa, The residual current of the modulated Bayard-Alpert gauge, Vacuum 36 (7–9) (1986) 559–560.
[64] V. Nemanic, M. Zumer, B. Zajec, The influence of a hot cathode vacuum gauge on the residual gas composition, Vacuum 70 (2003) 523–530.
[65] J. Völter, H. Berndt, K.D. Kramp, Bayard-Alpert-Manometer mit LaB_6-Kathode und kleiner Emission, Vakuum-Technik 16, Jhrg. Heft 1/2 (1967) 17–19.
[66] J.R. Dobrott, R.M. Oman, Ionisation gauge using a SiC p-n junction electron emitter, J. Vac. Sci. Technol. 7 (1) (1969) 214–215.
[67] K.E. Mc Culloh, C.R. Tilford, Nitrogen sensitivities of a sample of commercial hot cathode ionization gage tubes, J. Vac. Sci. Technol. 18 (1981) 994–996.
[68] C.R. Tilford, Sensitivity of hot cathode ionization gages, J. Vac. Sci. Technol. A 3 (1985) 546–550.
[69] J.L. Peters, Entwicklung und Betriebsverhalten einer neuen Ionisationsmanometer-Röhre, Vakuum-Technik 5, Jhrg. H. 4 (1969) 65–67.
[70] A. Van Oostrom, Trans. AVS Vac. Symp. (1961) 8443.
[71] J.C. Labrune, J.G. Theobald, A method for determining relative ionisation gauge sensitivities using cross section measurements, Vacuum 33 (3) (1983) 183–187.
[72] F. Watanabe, Comparative effects of gauge-wall materials on the outgassing rate of a hot cathode ionisation gauge, J. Vac. Sci. Technol. A 11 (2) (Mar/Apr 1993) 432–436.
[73] M. Hirata, M. Ono, H. Hojof, K. Nakayama, Calibration of secondary standard ionisation gauges, J. Vac. Sci. Technol. 20 (4) (April 1982) 1159–1161.
[74] W. Li, D. Zhang, Spherical oscillator gauge with field emission cold cathode, J. Vac. Sci. Technol. A 5 (4) (Jul/Aug 1987) 2376–2379.
[75] G. Messer, Verbesserung der Langzeitstabilität von Ionisationsvakuummetern durch Verwendung von Edelmetall-Ionenkollektoren, internal laboratory report, PTB, 1989.
[76] H. Gentsch, J. Tewes, G. Messer, An improved ion gauge with gold coated electrodes for reliable operation in reactive gases and for use as reference standard, Vacuum 35 (1985) 137–140.
[77] U. Harten, G. Grosse, H. Gentsch, Einfluß der Sekundärelektronenemission auf die Meßunsicherheit von Ionisationsvakuummetern, Wissenschaftliche Kurzberichte der Abteilung 9 (1986) 196. Institut Berlin.
[78] G. Grosse, U. Harten, W. Jitschin, H. Gentsch, Secondary electrons in ion gauges, J. Vac. Sci. Technol. (5) (Sep/Oct 1987) 3242–3243.
[79] R. Palme, Wolfram und Molybdän in der Vakuumtechnik, Glas- und Hochvakuum-Technik 7 (1952) 134–137.
[80] C.H. Edelmann, The influence of the hot cathode on the lower pressure limit of the bayard-alpert gauge, Exp. Tech. Phys. XXIII (5) (1975) 525–532.
[81] E. Gentsch, G. Gasser, Ionisation gauge as an inert system, Proc. 8th Int Vacuum Congress, Cannes 2 (1980) 203.
[82] F. Watanabe, Point collector ionisation gauge with spherical grid for measuring pressures below 10^{-11} Pa, J. Vac. Sci. Technol. A 5 (2) (Mar/Apr 1987) 242–248.
[83] C. Benvenuti, M. Hauer, Low pressure limit of the bayard-alpert gauge, Nucl. Instrum. Methods 140 (1977) 453–460.
[84] P.A. Redhead, Modulated bayard-alpert gauge, Rev. Sci. Instrum. (1960) 343–344.
[85] F. Watanabe, Ion spectroscopy gauge: total pressure measurements down to 10^{-12} Pa with discrimination against electron-stimulated-desorption ions, J. Vac. Sci. Technol. A 10 (5) (Sep/Oct 1992) 3333–3338.
[86] K.W. Yee, R.J. Carpenter, Regulation of ionisation gauge emission current to better than 0.05 %, Rev. Sci. Instrum. 34 (1963) 1101–1103.
[87] C.M. Spencer, D. Stäheli, High-Stability controller for Bayard-Alpert-Ionisation gauges, J. Vac. Sci. Technol. 5 (4) (1968) 105–108.
[88] N. Donkov, W. Knapp, Control of hot-filament ionisation gauge emission current: mathematical model and model based controller, Meas. Sci. Technol. 8 (1997) 798–803.
[89] P.J. Szwemin, The influence of the external circuit on the ionisation gauge stability, Vacuum 41 (7–9) (1990) 1807.
[90] B.R.F. Kendall, Ionisation gauge errors at low pressures, J. Vac. Sci. Technol. A 17 (4) (Jul/Aug 1999) 2041.
[91] P.J. Abbott, J.P. Looney, Influence of the filament potential wave form on the sensitivity of glass-envelope Bayard-Alpert gages, J. Vac. Sci. Technol. A 12 (5) (1994) 2911–2916.
[92] T.E. Madey, Summary abstract: surface phenomena and their influence on UHV gauges, J. Vac. Sci. Technol. A 5 (5) (1987) 3249.
[93] A.R. Baragiola, Principles and mechanisms of ion induced secondary electron emission, Nucl. Instrum. Methods B 78 (1993) 223–238.
[94] R.A. Baragiola, E.V. Alonso, A. Olivia-Florio, Electron emission from clean metal surfaces induced by low-energy light ions, Phys. Rev. B 19 (1979) 121.
[95] H.P. Winter, F. Aumayr, C. Lemell, J. Burgdörfer, S. Lederer, H. Winter, Kinetic electron emission by grazing atom scattering from clean flat metal surfaces, Nucl. Instrum. Methods B 256 (2007) 455–463.
[96] G. Lakits, F. Aumayr, M. Heim, H. Winter, Threshold of ion-induced kinetic electron emission from a clean metal surface, Phys Rev A 42 (9) (1990) 5780–5783.
[97] H.D. Hagstrum, Auger ejection of electron from tungsten by noble gas ions, Phys. Rev. 96 (2) (1954) 325–335.
[98] H.D. Hagstrum, Theory of auger ejection of electrons from metals by ions, Phys. Rev. 96 (2) (1954) 336–365.
[99] H.D. Hagstrum, Auger ejection of electron from tungsten by noble gas ions, Phys. Rev. 104 (2) (1956) 317–318.
[100] H.D. Hagstrum, Effect of monolayer adsorption on the ejection of electrons from metals by ions, Phys. Rev. 104 (6) (1956) 1516–1527.
[101] L.M. Kishinevsky, Estimation of electron potential emission yield dependence on metal and ion parameters, Radiat. Eff. 19 (1) (1973) 23–27.
[102] R.A. Baragiola, E.V. Alonso, J. Ferron, A. Olivia-Florio, Ion-induced electron emission from clean metals, Surf. Sci. 90 (1979) 240–255.
[103] A.V. Phelps, Z. Lj Petrović, Cold-cathode discharges and breakdown in argon: surface and gas phase production of secondary electrons, Plasma Sources Sci. Technol. 8 (1999) R21–R44.
[104] P. Varga, H. Winter, Slow particle-induced electron emission from surfaces, in: D. Hasselkamp, K.O. Rothard, J.K. Groeneveld (Eds.), Particle Induced Electron Emission II, Springer Verlag, Berlin Heidelberg, 1992.
[105] G. Lakits, F. Aumayr, M. Heim, H. Winter, Threshold for ion-induced kinetic electron emission from a clean metal surface, Phys Rev A 49 (9) (1990) 5780–5783.
[106] U. Fano, W. Lichten, Interpretation of Ar^+-Ar collisions at 50 keV, Phys. Rev. Lett. 14 (1965) 627.
[107] M. Barat, W. Lichten, Extension of the electron-promotion model to asymetric atomic collisions, Phys Rev A 6 (1972) 211.
[108] N. Bajales, S. Montoro, E.C. Goldberg, R.A. Baragiola, J. Ferron, Identification of mechanisms of ion induced electron emission by factor analysis, Surf. Sci. 579 (2005) L97–L102.
[109] H.U. Becker, G. Messer, Sensitivity dependence on collector surface properties in ion gauges, Proc. 8th Int. Vacuum Congress, Cannes II (1980) 234–237.
[110] U. Harten, G. Grosse, W. Jitschin, H. Gentsch, Surface effects on the stability of hot cathode ionisation gauges, Vacuum 38 (1988) 167–169.

[111] C.P. Gopalaraman, R.A. Armstrong, P.A. Redhead, Sensitivity variations in Bayard-Alpert gauges caused by Auger emission at the collector, J. Vac. Sci. Technol. 7 (1) (1970) 195–198.
[112] R.P.W. Lawson, G. Carter, Inert gas bombardment induced work function changes in polycrystalline tungsten and gold ribbon, Vacuum 18 (4) (1968) 205–211.
[113] M. Kudo, Y. Sakai, T. Ichinokawa, Dependencies of secondary electron yields on work function for metals by electron and ion bombardment, Appl. Phys. Lett. 76 (2000) 3475.
[114] R.D. Ramsier, J.T. Yates Jr., Electron-stimulated desorption: principles and applications, Surf. Sci. Rep. 12 (1991), 243–378.
[115] D. Menzel, B. Gomer, J. Chem. Phys. 41 (1964) 3311.
[116] P.A. Redhead, Interaction of slow electrons with chemisorbed oxygen, Can. J. Phys. 42 (1964) 886–905.
[117] M.L. Knotek, P.J. Fiebelman, Ion desorption by core-hole Auger decay, Phys. Rev. Lett. 40 (14) (1978) 964–967.
[118] H. Niehus, Angular resolved ESD for surface structure determination, Appl. Surf. Sci. 13 (1982) 292–309.
[119] S. Prigge, H. Niehus, E. Bauer, Electron stimulated desorption ion energy distribution and surface structure: O on W (100), Surf. Sci. 75 (1978) 635–656.
[120] M. Takizawa, A. Yoshimi, T. Katunuma, T. Yabe, C. Oshima, Electron stimulated desorption ions of hydrogen and deuterium molecules in extremely high vacuum, Vacuum 47 (1996) 571–573.
[121] P.A. Redhead, Ion desorption by electron bombardment; relation to total and partial pressure measurement, J. Vac. Sci. Technol. 7 (1) (1970) 182–187.
[122] P.A. Redhead, The effects of adsorbed oxygen on measurement with ionisation gauges, Vacuum 13 (1963) 253–258.
[123] F. Watanabe, Investigation and reduction of spurious peaks caused by electron-stimulated desorption and outgassing by means of a grid heating method in a hot cathode quadrupole residual gas analyzer, J. Vac. Sci. Technol. A 20 (5) (2002) 1222–1229.
[124] F. Watanabe, Bent belt-beam gauge: extending low-pressure measurement limits in a hot-cathode ionization vacuum gauge by combining multiple methods, J. Vac. Sci. Technol. A 28 (3) (2010) 486–494, https://doi.org/10.1116/1.3400233.
[125] F. Watanabe, M. Suemitsu, Separation of electron-stimulated-desorption neutrals from outgassing originated from the grid surface of emission-controlled gauges: studies with a heated-grid gauge, J. Vac. Sci. Technol. A 17 (1999) 3467–3472.
[126] F. Watanabe, Hysteresis of electron-stimulated desorption in an ion spectroscopy gauge, Vacuum 47 (6–8) (1996) 583–586.
[127] F. Watanabe, Dominance of electron-stimulated desorption neutral species in ultra-high vacuum pressure measurements, Vacuum 52 (1999) 333–338.
[128] F. Watanabe, H. Ishimaru, Ion current modulation of a residual gas analyzer, J. Vac. Sci. Technol. A 3 (1985) 2192.
[129] H. Seiler, Secondary electron emission in the scanning electron microscope, J. Appl. Phys. 54 (1983) R1–R18.
[130] R.F. Egerton, Electron-Energy Loss Spectroscopy in the Electron Microscope, third ed., Springer, New York, 2011.
[131] V. Baglin, J. Bojko, O. Gröbner, B. Henrist, N. Hilleret, C. Scheuerlein, M. Taborelli, The secondary electron yield of technical materials and its variation with surface treatments, Proc. EPAC (2000) 217–221. Vienna.
[132] J.G. Werner, J.H. Leck, The operation of the hot cathode ionisation gauge in hydrogen, Vacuum 19 (7) (1969) 317–318.
[133] G. Grosse, U. Harten, W. Jitschin, H. Gentsch, Secondary electrons in ion gauges, J. Vac. Sci. Technol. A 5 (5) (1987) 3242–3243.
[134] J.N. Smith, W. Fite, Reflection and dissociation of H_2 in tungsten, J. Chem. Phys. 37 (4) (1962) 898–904.
[135] K.F. Poulter, J.A. Pryde, Chemisorption of hydrogen on rhenium, Br. J. Appl. Phys. 2 (1) (1968) 169–172.
[136] E.H. Hirsch, Surface ionisation on tungsten in a varying ambient atmosphere, Vacuum 85 (2010) 373–379.
[137] A. Berman, Methods of pumping speed and gas release measurement in ionisation gauge heads - a review, Vacuum 32 (8) (1982) 497–508.
[138] A. van Oostrom, Totaldruckmessung nach dem Ionisationsprinzip und ihre Störeffekte, Vakuum-Technik 16 (7) (1967) 159–167.
[139] G. Moraw, The influence of ionisation gauges on gas flow measurements, Vacuum 24 (3) (1974) 125–128.
[140] F. Nakao, Determination of the ionisation gauge sensitivity using the relative ionisation cross-section, Vacuum 25 (9) (1975) 431–435.
[141] R. Holanda, Investigation of the sensitivity of ionisation-type vacuum gauges, J. Vac. Sci. Technol. 10 (6) (1973) 1133–1139.
[142] F.W. Lampe, J.F. Franklin, F.H. Field, Cross Sections for Ionization by Electrons, J. Am. Chem. Soc. 79 (1957) 6129–6132.
[143] J.E. Bartmess, R.M. Georgiadis, Empirical methods for determination of ionisation gauge relative sensitivities for different gases, Vacuum 33 (3) (1983) 149–153.
[144] R.L. Summers, Empirical Observations on the Sensitivity of Hot Cathode Ionisation Type Vacuum Gauges, 1969. NASA Technical Note TN D-5285, Washington D.C.
[145] T.A. Flaim, P.D. Ownby, Observations on Bayard-Alpert Ion gauge sensitivities to various gases, J. Vac. Sci. Technol. 8 (5) (1971) 661–662.
[146] A.R. Filippelli, S. Dittmann, Search for pressure dependence in the sensitivity of several common types of hot-cathode ionisation gauges for total pressures down to 10^{-7} Pa, J. Vac. Sci. Technol. A 9 (5) (1991) 2757.
[147] C.R. Tilford, K.E. McCulloh, H.S. Woong, Performance characteristics of a broad range ionisation gauge tube, J. Vac. Sci. Technol. A 20 (4) (1982) 1140–1143.
[148] K. Jousten, P. Röhl, Comparison of the sensitivities of ionisation gauges to hydrogen and deuterium, Vacuum 46 (1995) 9–12.
[149] D. Li, K. Jousten, Comparison of some metrological characteristics of hot and cold cathode ionisation gauges, Vacuum 70 (2003) 531–541.
[150] H. Yoshida, K. Arai, Quantitative measurements of various gases in high and ultrahigh vacuum, J. Vac. Sci. Technol. A 36 (2018), 031604, https://doi.org/10.1116/1.5018210.
[151] S.D. Wood, C.R. Tilford, Long-term stability of two types of hot cathode ionisation gauges, J. Vac. Sci. Technol. A 3 (3) (1985) 542–545.
[152] A.R. Filippelli, P.J. Abbott, Long-term stability of Bayard-Alpert gauge performance: results obtained from repeated calibrations against the NIST primary vacuum standard, J. Vac. Sci. Technol. A 13 (5) (1995) 2582–2586.
[153] J.A. Fedchak, D.R. Defibaugh, Long-term stability of metal-envelope enclosed Bayard-Alpert ionisation gauges, J. Vac. Sci. Technol. A 30 (6) (2012), 061601.
[154] K.F. Poulter, Vacuum gauge calibration by the orifice-flow method in the pressure range 10^{-4} Pa to10 Pa, Vacuum 28 (1978) 135.
[155] K.F. Poulter, C.M. Sutton, Long term behaviour of ionization gauges, Vacuum 31 (1981) 147–150.
[156] I. Warshawsky, A report from the AVS Standards Committee: Comparison of ion gauge calibrations by several standards laboratories, J. Vac. Sci. Technol. 20 (1982) 75.
[157] H. Yoshida, K. Arai, H. Akimichi, M. Hirata, Stability tests of ionization gauges using two-stage flow-dividing system, Vacuum 84 (2010) 705–708.
[158] H. Yoshida, H. Akimichi, M. Hirata, Calibration of ultrahigh vacuum gauge from 10^{-9} Pa to 10^{-5} Pa by the two-stage flow-dividing system, Vacuum 86 (2011) 226–231.
[159] H. Yoshida, et al., Report of pilot study CCM.P P1 for international comparison of absolute pressure measurements in gas from 3×10^{-9} Pa to 9×10^{-4} Pa, Metrologia 52 (1A) (2015), 07012-07012.
[160] K. Jousten, A.R. Filipelli, C.R. Tilford, F.J. Redgrave, Comparison of the standards for high and ultrahigh vacuum at three national standard laboratories, J. Vac. Sci. Technol. A 15 (4) (1997) 2395–2406.
[161] D. Li, et al., Vacuum-calibration apparatus with pressure down to 10^{-10} Pa, J. Vac. Sci. Technol. A 28 (2010) 1099–1104, https://doi.org/10.1116/1.3457934.
[162] P.J. Abbott, J.P. Looney, P. Mohan, The effect of ambient temperature on the sensitivity of hot cathode ionisation gauges, Vacuum 77 (2005) 217–222.
[163] C.R. Tilford, A.R. Filippelli, P.J. Abbott, Comments on the stability of Bayard–Alpert ionisation gages, J. Vac. Sci. Technol. A 13 (2) (1995) 485–487.
[164] J.P. McFadden, M. Wüest, Raytracing in instrument design, in: M. Wüest, D. S. Evans, R. von Steiger (Eds.), Calibration of Particle Instruments in Space Physics, ISSI Scientific Report, SR-007, ESA Publications Division, The Netherlands, 2007.
[165] D.A. Dahl, J.E. Delmore, A.D. Appelhans, Simion PC/Ps2 electrostatic lens design program, Rev. Sci. Instrum. 61 (1) (1990) 607–609.
[166] D.A. Dahl, SIMION for the personal computer in reflection, Int. J. Mass Spectrom. 200 (2000) 3–25.
[167] R. Kauert, O.F.O. Kieler, St Biehl, W. Knapp, Chr Edelmann, St Wilfert, Numerical investigations of hot cathode ionisation gauges, Vacuum 51 (1) (1998) 53–59.
[168] P. Sauter, Entwicklung einer Monte-Carlo Simulation zum Verständnis des ASDEX pressure gauge, Max-Planck-Institut für Plasmaphysik, IPP –Report, IPP 10/37 (2008).
[169] P. Juda, B. Jenninger, P. Chiggiato, T. Richard, 3D-simulation of ionisation gauges and comparison with measurements, Vacuum 138 (2017) 173–177.
[170] D.J. Turner, C. Priestland, Sensitivity variations in the Bayard-Alpert ionisation gauge, Part two: simulation of ion collection, for collimated beam input and chaotic gas input, using a digital computer, Vacuum 18 (6) (1968) 319–326.
[171] J. Kudzia, W. Slowko, Numerical method of calculating ion current in a high pressure ionisation gauge, Vacuum 31 (8–9) (1981) 359–361.
[172] A. Schopphoff, Konzeption und Test eines modifizierten Extractor-Ionisationsvakuummeters, Diplomarbeit, Fachbereich Naturwissenschaften I – Physik, Bergische Universität, Gesamthochschule Wuppertal, WU D 94-20.
[173] R. Silva, N. Bundaleski, Ana L. Fonseca, O.M.N.D. Teodoro, 3D-Simulation of a Bayard Alpert ionisation gauge using SIMION program, Vacuum 164 (2019) 300–307.
[174] L.G. Pittaway, Electron trajectories in ionisation gauges, J. Phys D 3 (1970) 1333.